Princeton/$\mu\mu$/00-30
K.T. McDonald
December 1, 2000

Magnetohydrodynamics of a Pulsed Mercury Jet Entering a Solenoid at an Angle

Abstract

This note is an update of secs. 2.1-5 of the E951 proposal [1].

1 A Targetry Scenario for a Muon Collider and a Neutrino Factory

Figure 1 gives an overview of the configuration for production of pions by a proton beam impinging on a long, thin target, followed by capture of low-momentum, forward pions in a channel of solenoid magnets with rf cavities to compress the bunch energy while letting the bunch length grow, thus rotating the bunch in phase space. This configuration was conceived for a muon collider [2, 3] with a 4-MW proton beam, and is similar to that being considered for a neutrino factory based on a muon storage ring [4, 5].

1.1 Pion Production

To achieve the present design luminosity of 7×10^{34} cm^{-2}s^{-1} for a 3-TeV CoM muon collider (or 10^{31} cm^{-2}s^{-1} at 100-GeV CoM), 2×10^{12} (or 4×10^{12} at 100-GeV CoM) muons of each sign must be delivered to the collider ring in each pulse at 15 Hz. We estimate that a muon has a probability of only 1/4 of surviving the processes of cooling and acceleration, due to losses in beam apertures or by decay. Thus, 0.8×10^{13} muons (1.6×10^{13} at 100 GeV) must exit the phase-rotation channel each pulse. For pulses of 2.5×10^{13} protons (5×10^{13} for 100 GeV), this requires 0.3 muons per initial proton. And since the efficiency of the phase-rotation channel is about 1/2, this is equivalent to a capture of about 0.6 pions per proton, a very high efficiency.

The pions are produced by the interaction of the proton beam with the primary target. Extensive simulations have been performed for pion production from 8-30-GeV proton beams on different target materials in a high-field solenoid [2, 6, 7, 8, 9]. Three different Monte Carlo codes [10, 11, 12, 13] predict similar pion yields despite significant differences in their physics models. The Collaboration is involved in an AGS experiment [14] to measure the yield of very low momentum pions, which will validate the codes in the critical kinematic region. Further studies of pion production are underway at CERN [15].

For proton beam energies above 8 GeV, the pion yield is greater for relatively high-Z materials, and for these, the pion yield is maximal for longitudinal momenta of the same order as the average transverse momentum (≈ 200 MeV/c). Targets of varying composition ($6 <$

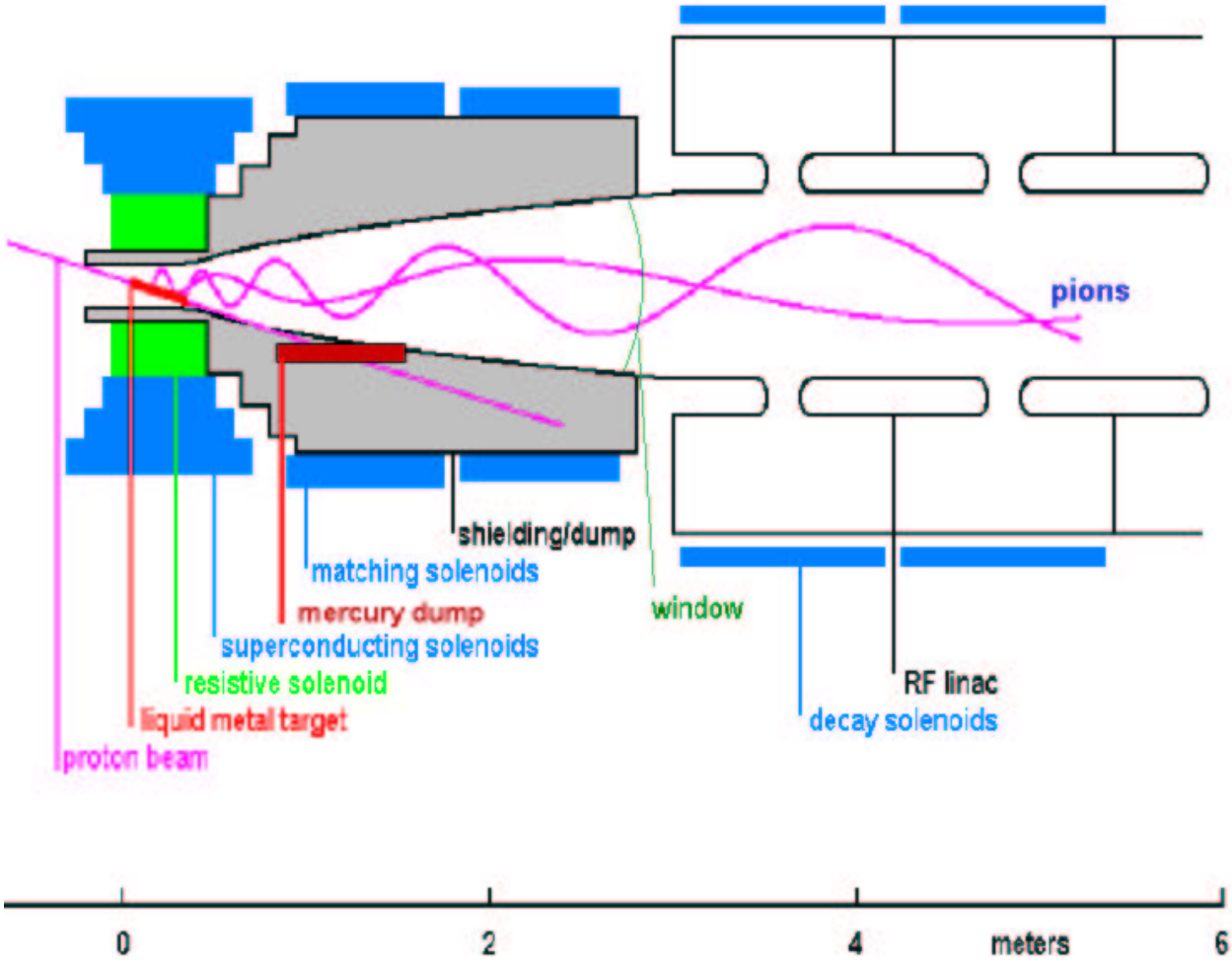

Figure 1: Schematic view of pion production, capture and initial phase rotation. A pulse of 16-30 GeV protons is incident on a skewed target inside a high-field solenoid magnet followed by a decay and phase-rotation channel.

$Z < 82$), radii (0.2-3 cm) and thicknesses (0.5-3 nuclear interaction lengths, λ_I) have been explored. For a fixed number of interaction lengths, the pion yield per proton rises almost linearly with proton energy [9], and hence is almost proportional to the energy deposited in the target. The yield is higher for medium and high-Z target materials, with a noticeable gain at $Z > 26$ for 30-GeV proton beams, but with only a minor effect for $E \leq 16$ GeV, as shown in Fig. 2a.

1.2 Target

The target should be 2-3 interaction lengths long to maximize pion production. A high-density, high-Z material is favored to maximize pion production (for beam energies above 8 GeV) and to reduce the target length, thereby minimizing the size and cost of the capture solenoid magnet. Target radii larger than about 1 cm lead to lower pion rates due to

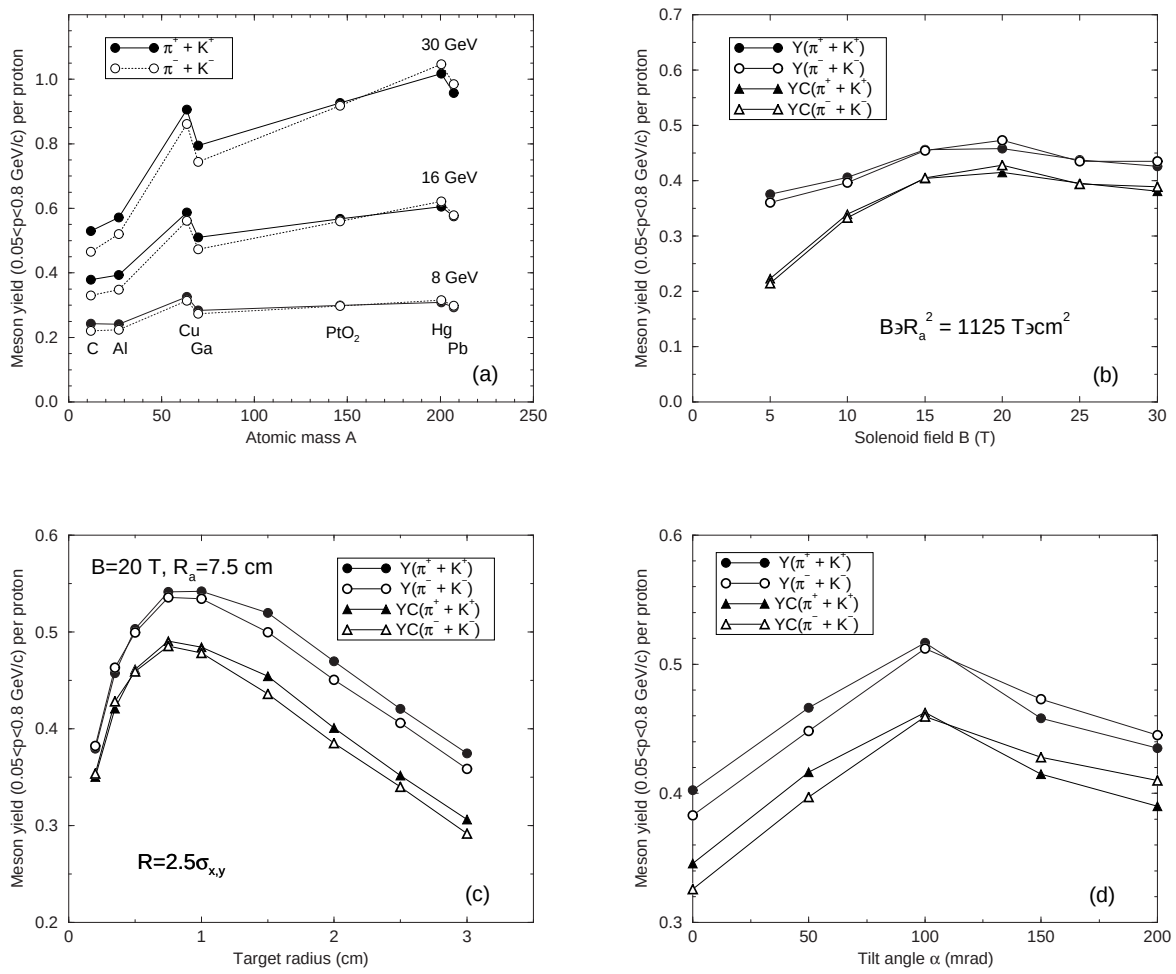

Figure 2: a) Meson yield $(\pi + K)$ from a 1.5-λ_I, 1-cm-radius target irradiated with 8, 16 and 30-GeV proton beams as a function of target atomic mass; b) Meson yield from a 3-λ_I, 1-cm-radius gallium target tilted at angle 150 mrad in a 16-GeV proton beam *vs.* solenoid field for a fixed adiabatic invariant BR_a^2; c) Meson yield as a function of target radius; d) Meson yield *vs.* tilt angle between the axis of the capture solenoid and the proton beam. The target is aligned along the beam. The curves labeled YC show mesons that are transported into the decay channel.

reabsorption, while smaller diameter targets reduce the added production from secondary interactions. Tilting the target by 100-150 mrad minimizes the loss of pions by absorption in the target after one or more turns on their helical trajectory. Another advantage of the tilted target geometry is that the high-energy and neutral components of the shower can be absorbed in a water-cooled beam dump below the magnetic axis (see Fig. 1).

About 30 kJ of energy is deposited in a high-Z target by each proton pulse of a 4-MW beam (10% of the beam energy). Hence, the target absorbs 400 kW of power at the 15-Hz pulse rate. Cooling of the target via contact with a thermal bath would lead to unacceptable absorption of pions, and radiative cooling is inadequate for such high power in a compact

target. Therefore, the target must move so as to carry the energy deposited by the proton beam to a heat exchanger outside the solenoid channel.

Both moving-solid-metal and flowing-liquid targets have been considered, with the latter as the currently preferred solution. A liquid is relatively easy to move, easy to cool, can be readily removed and replaced, and is the preferred target material for most spallation neutron sources under study. A liquid flowing in a pipe was considered, but experience at CERN [16] and Novosibirsk [17] indicates that shock damage to the pipe is a serious problem. Therefore, an open liquid jet is proposed.

A jet of liquid mercury has been demonstrated [18] (see Fig. 3) but not exposed to a beam. While mercury is presently the leading candidate for a liquid metal target, its low boiling point may lead to operational difficulties at high beam power. Hence, low-melting-point lead alloys, and even gallium alloys despite their lower density, are also being considered.

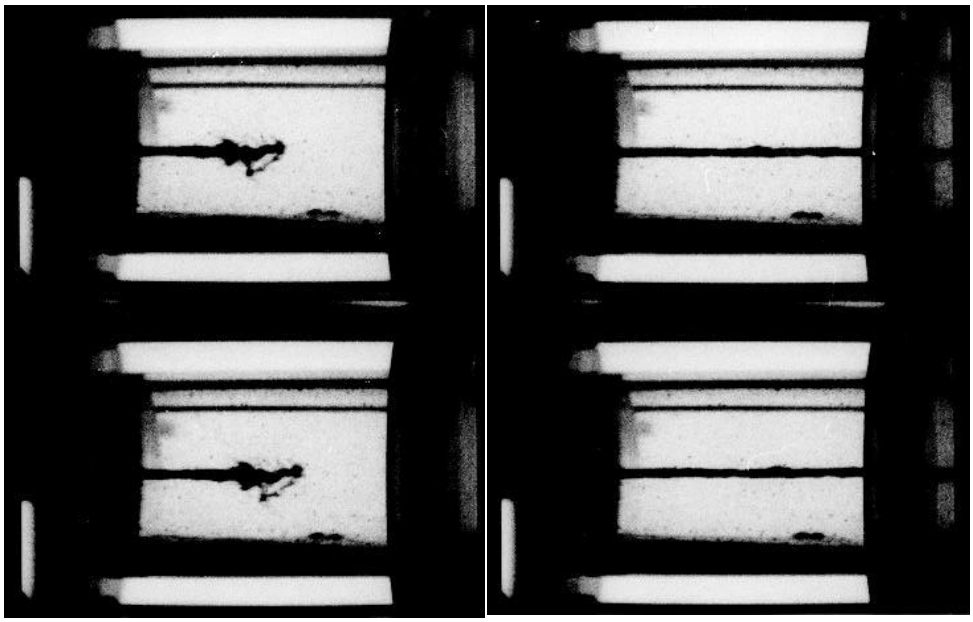

Figure 3: Photographs of a 3-mm-diameter mercury jet [18].

It is expected that the jet will disperse after being struck by the beam. The target station must survive damage resulting from the violence in this dispersion. This consideration will determine the minimum beam, and thus jet, radius.

For a conducting liquid jet in a strong magnetic field, as proposed, strong eddy currents will be induced in the jet, causing reaction forces that may disrupt its flow [20, 21, 22, 23, 24, 25, 26, 27, 28]. The forces induced are proportional to the square of the jet radius, and set a maximum for this radius of order 5-10 mm. If this maximum is smaller than the minimum radius set by shock considerations, then multiple smaller beams and jets could be used; *e.g.*, four jets of 5 mm radius with four beams with 2.5 10^{13} protons per bunch.

Liquid targets made from insulating materials such as liquid PtO_2 or Re_2O_3, slurries (*e.g.*, Pt in water), or powders [29] would have minimal eddy-current effects. However, the intense proton beam would rapidly decompose and chemical compound, and the flow properties of slurries and powders do not appear favoable enough to warrant further consderation.

A moving-solid-metal target is not the current baseline solution, but is a serious consideration. In this case [30, 31, 32], the target could consist of a long flat band or hoop of copper-nickel that moves along its length (as in a band saw). The band would be many meters in length, would be cooled by gas jets away from the target area, and would be supported and moved by rollers, as shown in Fig. 4.

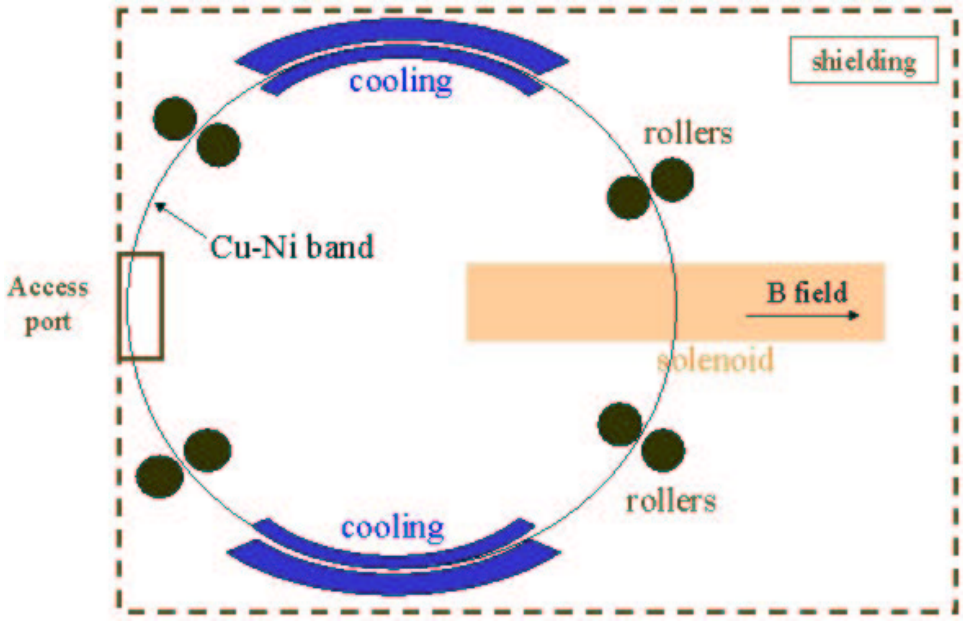

Figure 4: Alternative concept of a solid metal target in the form of a rotating Cu-Ni band [30].

In view of the technical uncertainties associated with moving targets, liquid or solid, a stationary, radiatively cooled carbon target has also been considered [33, 34, 35, 36, 37].

2 Solid or Liquid Target?

The muons of a muon collider will arise from the decay of pions produced in the interaction of some 1.5×10^{15} protons/s on a primary target. If these protons have 16-GeV energy, the beam power is 4 MW. The target will be about 2 interaction lengths long and will absorb about 10% of the beam power, *i.e.*, about 400 kW. The beam repetition rate is 15 Hz, so each beam pulse deposits about 30 kJ of energy in the target.

2.1 Cooling the Target

The target is in the form of a cylinder, about 1 cm in radius, 30 cm in length, with a volume of about 100 cm^3. If the target material has density 10 g/cm^3, then the target mass is about 1 kg. Thus the beam-energy deposition in the target averages about 30 J/g. Taking the heat capacity of a typical metal as 0.2 J/(g-°K), the temperature rise of a metallic target is about 150°K per pulse. If the target were not cooled, it would melt (if solid) or boil (if liquid) after a dozen or so beam pulses.

However, the goal of collecting the maximal number of muons per proton is not consistent with typical cooling schemes in which the target material is in immediate contact with a large thermal reservoir.

Radiative cooling of the target appears to be unfeasible. The power radiated by a surface of area A and emissivity ϵ at temperature T is $\epsilon\sigma T^4 A$, where $\sigma = 5.67 \times 10^{-12}$ J/(cm^2(°K)^{4}s) is the Stefan-Boltzmann constant. The emissivities of typical metals are only about 0.2 (in contrast to carbon, with $\epsilon \approx 0.8$). The surface area of the target cylinder is about 200 cm^2. At 2000°K, the radiated power would be only 3.6 kW, well shy of the 400-kW beam load.

Thus, we are led to consider scenarios in which the target is in motion, with any subunit of the target exposed to only one or a few beam pulses before being transported away from the interaction region, to be cooled by a remote thermal reservoir. For similar reasons, targets at multimegawatt neutron spallation sources are expected to be based on flowing liquid metal, usually mercury [38, 39, 40, 41, 42, 43, 44].

2.2 Thermal Shock

The simplest option would be use of a flowing liquid metal contained within a (static) metal pipe [46, 47, 48]. However, when a large pulse of energy is deposited in a material in a time that is short compared to the transit time of a sound wave (≈ 3 μs/cm), a pressure (stress) wave results [35, 36, 49, 50, 40, 51, 52, 53, 54, 55]. Since the proton pulse for a muon collider is expected to be only about 2 ns long, stress waves will be excited in the target, and consequent damage to the target and adjacent material is a concern.

This issue is often called "thermal shock". The pressure wave front propagates outwards at roughly the speed of sound in the target material. However, thermal shock is not necessarily associated with bulk transport of matter at the speed of sound.

2.2.1 The Initial Pressure Wave.

If the beam-induced stress exceeded the tensile strength of the target material, the latter would fracture.

We present a simplified model to estimate the regime in which a pressure wave will "tear" the target apart, whether solid or liquid (see also refs. [49, 56]). When an energy density ΔU (per gram) is deposited quickly in the target, we first calculate the temperature change ΔT that would occur, assuming no thermal diffusion. Then, we calculate the strain, $\Delta l/l$ corresponding to that ΔT, and evaluate the stress P corresponding to that strain. Tearing is likely to occurs if the stress exceeds the tensile strength. In this model, tearing occurs during the phase of the pressure wave when the material is under tension, *i.e.*, for negative pressure. In liquids, this phenomenon is called cavitation [57, 58, 59, 60].

We suppose that the effective tensile strength of a liquid metal is similar to that of the same metal in solid form. For example, the tensile strength of sea ice is reported as about 8 atm [61], while that of water can exceed 200 atm in a static measurement [62] but was measured as 8 atm by an explosive technique [63] that has much in common with the present concerns; see also [57, 58].

For most metals, the tensile strength (pressure) P is about 0.002 of the modulus of elasticity E (Young's modulus). Thus,

$$\Delta U = C\Delta T = \frac{C}{\alpha}\frac{\Delta l}{l} = \frac{C}{\alpha}\frac{P}{E} \approx 0.002\frac{C}{\alpha}, \tag{1}$$

where C is the heat capacity, α is the coefficient of thermal expansion, and the approximation holds on setting the stress equal to the tensile strength. If, for example, the heat capacity is $C = 0.3$ J/g-°C, and $\alpha \approx 2 \times 10^{-5}$/°C, then we expect the target material will tear when $\Delta U \approx 30$ J/g. This is very nearly the expected energy deposition in the muon-collider target. It is, however, somewhat smaller than a semi-empirical value of 200 J/g for the threshold for thermal-shock damage [64].

If the target tears, it is possible that the fragments do damage to the surrounding vessel. If all the deposited energy were converted to kinetic energy and the target fragmented completely, then the velocity of the fragments would be $\sqrt{2\Delta U} \approx 8$ m/s for $\Delta U = 30$ J/g. A model of spray velocities in explosions of liquids [63] leads to similar values. Studies of an exploding mercury jet were performed safely inside a plastic vessel whose wall was only $1/4''$ thick [65, 66, 67]. Thus, it is encouraging that if a liquid target were dispersed into droplets by the beam, the droplets would do little damage to the surrounding vessel. However, this should be confirmed by experiment.

2.2.2 The Reflected Pressure Wave.

Even if target parameters are chosen such that the initial pressure wave does not tear the material, there is another concern. When the pressure wave reaches the surface of the target, it will, in general, be reflected. In the case of a cylindrical target, the reflected wave converges on the axis of the target and will typically result in higher peak pressures than exist in the initial outgoing wave. Hence, there is a serious prospect for localized fracture or vaporization of the target material close to the target axis, whether the cylindrical target is solid or liquid. In the case of a liquid, this is likely to induce localized damage to the target pipe, particularly on the upstream wall.

The destructive effects of pressure waves and cavitation on liquid-metal targets in pipes have been demonstrated at the CERN ISOLDE facility [16, 68], as shown in Figs. 5-6, and also at the Budker Institute [17], as shown in Fig. 7. Practical targets based on liquid metals in pipes require sufficiently long beam pulses and/or target geometries (*e.g.*, planar) in which imploding pressure waves do not occur. Therefore, liquids in pipes are not considered further for a muon-collider target. Likewise, a moving solid cylindrical target is very problematic at a muon collider.

Figure 5: Full-scale model of an ISOLDE target consisting of a 2-cm-diameter, 20-cm-long tantalum cylinder containing molten lead.

Figure 6: Photograph of an ISOLDE liquid-lead target that ruptured around the upstream window after a few beam pulses [16].

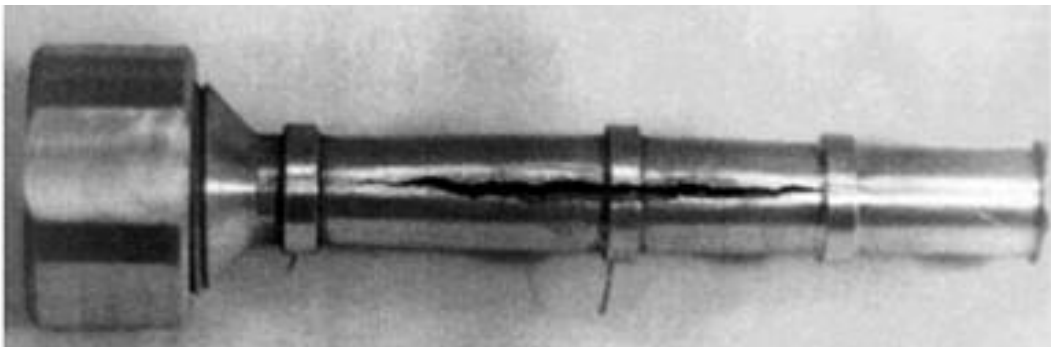

Figure 7: Photograph of a mercury target contained in an aluminum cylinder that ruptured after exposure to a beam that deposited 1 kJ/g per pulse [17].

2.3 Muon-Collider Primary-Target Options

The remaining options for the muon-collider target are a free, cylindrical liquid-metal jet or a moving planar solid target, as have been sketched in Figs. 1 and 4. The baseline design to be studied in the proposed R&D program utilizes a free liquid-metal jet. The moving band target presently is considered as the backup option.

2.4 Additional Issues for a Solid Target

As well as surviving the thermal-shock of each beam pulse, a solid target must survive the long-term effects of radiation damage. These include embrittlement, swelling and even fracture of the material due to displacement damage and hydrogen/helium production [69]. The immunity of a liquid target to these effects is an argument in favor of that option.

The cross section for displacement of a target atom in a 16-30-GeV proton beam is about 10^{-24} m^2. In an operational year of 10^7 s, a beam of 1.5×10^{15} proton/s whose rms radius is nominally 4 mm results in about 300 displacements per atom (dpa) in a nonmoving target.

For a moving solid target, any given atom is exposed to a proton flux that is less than the total by the factor

$$\frac{L_{\rm int} N_{\rm overlap}}{L_{\rm total}}, \tag{2}$$

where $L_{\rm int}$ is the length of the interaction region ($\approx$ 30 cm), $L_{\rm total}$ is the total length of the target material ($\approx$ 30 m, say), and $N_{\rm overlap}$ is the number of adjacent beam pulses that irradiate a given region. That is,

$$N_{\rm overlap} = \frac{L_{\rm int} f}{v}, \tag{3}$$

for a target moving with velocity v along the beam whose pulse rate is f Hz. For example, with $v = 1$ m/s and $f = 15$ Hz, then $N_{\rm overlap} \approx 5$, and each part of the moving target experiences only 5% of the exposure of a nonmoving target, namely about 15 dpa in a year of operation. This still corresponds to significant radiation damage, suggesting that the target band would need to be replaced several times a year. The viability of a moving solid target needs further investigation.

There is little available evidence as to the mechanical properties of targets after such exposures. A series of studies of solid targets at CERN generally indicated severe mechanical damage to intensely irradiated targets [70, 71, 72, 73, 74, 75], although the damage was due to a combination of single-pulse shock as well as radiation. Nickel targets appear to survive well for energy depositions up to a large fraction of the shock-damage threshold [76]. Copper targets appear to form excessive amounts of copper sulfate if irradiated in contact with air [77].

3 Beam-Induced Radioactivity

The high flux of protons into the target will induce some radioactivity no matter what the target consists of. A thorough study of this issue will be needed before a final decision as to the target material is taken. A first study will be made using a MARS simulation of the hadronic cascade in the target.

For any target material with an atomic number greater than or equal to that of mercury, radioactive isotopes of mercury will emerge in the vapor phase [78]. These are only the most prominent among other radioactive vapors that will be produced. Hence, a high-Z target at a muon-collider source must be enclosed in a gas-tight system that includes capture tanks for the vapors, including those exhausted from any pumps. This proposal does not cover R&D towards such a system, which would be modeled after the target-containment system at the ISOLDE facility at CERN.

Especially high levels of activity would arise for targets containing bismuth, due to the sequence:

$$\text{Low-energy neutron} + \mathrm{Bi}^{209}_{83} \rightarrow \mathrm{Bi}^{210}_{83} + \gamma, \qquad \mathrm{Bi}^{210}_{83} \rightarrow \mathrm{Po}^{210}_{84} + \beta^- \quad (\text{half life} = 5 \text{ days}). \tag{4}$$

Po^{210} has a half life of 135 days and decays primarily via a 5.3-MeV α, but has a 0.1% branch to an 803-keV x-ray.

If, say, every beam proton results in one transmutted Bi atom, then the steady-state Po population would be equal to the total flux of protons in 135 days: $135 \times 10^5 \times 10^{15} \approx 10^{22}$ atoms, assuming a proton flux of 10^{15}/s. The number of Po decays would be 10^{15}/s in the steady state, *i.e.*, about 30,000 curies!

The α-particles will be almost entirely absorbed in the target, but the 800-keV x-rays present more of a problem. The steady-state strength of the x-rays corresponds to about 30 curies (assuming each beam proton results in one Po atom).

However, the resulting polonium would be dissolved in the liquid of the target with very low probability of being in vapor molecules. Hence, the handling of an activated bismuth alloy would be relatively straightforward and little more difficult than for other target materials [79].

4 Candidate Liquid Metals

Liquid metals have long been used as coolants for nuclear reactors, and a useful summary of candidate materials has been given by Lyon [80]. Table 1 presents a brief survey of

low-melting-temperature metals, and Table 2 list some relevant physical properties of the elements of candidate materials.

Table 1: Survey of low-melting-temperature metals [80].

Approximate melting point, °C	Approximate composition, wt %
185	48 bismuth, 52 thallium (eutectic)
180	38 lead, 62 tin (eutectic)
140	60 bismuth, 40 cadmium (eutectic)
140	58 bismuth, 42 tin (eutectic)
130	56 bismuth, 40 tin, 4 zinc (eutectic)
125	44.5 bismuth, 55.5 lead (eutectic)
120	25 cadmium, 75 indium (eutectic)
117	48 tin, 52 indium (eutectic)
105	48 bismuth, 28.5 lead, 14.5 tin, 9.0 antimony (matrix alloy)
93	50 bismuth, 25 lead, 25 tin
91.5	51.6 bismuth, 40.2 lead, 8.2 cadmium (eutectic)
71.7-69.7	50 bismuth, 25 lead, 12.5 tin, 12.5 cadmium (Wood's metal)
70	33 bismuth, 67 indium (eutectic)
70	50 bismuth, 26.7 lead, 13.3 tin, 10 cadmium (eutectic)
60.5	32.5 bismuth, 16.5 tin, 51 indium
58.2	49.5 bismuth, 17.6 lead, 11.6 tin, 21.3 indium
46.5	40.63 bismuth, 22.11 lead, 10.65 tin, 8.2 cadmium, 18.1 indium
33	32 potassium, 68 rubidium (eutectic)
17	12 tin, 6 zinc, 82 gallium (eutectic)
10.8	12.5 tin, 17.6 indium, 69.8 gallium (eutectic)
10.7	16 tin, 21.5 indium, 62.5 gallium (eutectic)
−8	8 sodium, 92 rubidium (eutectic)
−11	22 sodium, 78 potassium (eutectic)
−30	5 sodium, 95 cesium (eutectic)
−40	87 cesium, 13 rubidium (eutectic)
−48	23 potassium, 77 cesium (eutectic)

We are interested in high-Z, high-density target materials for the most-efficient pion production. High electrical resistivity is helpful in reducing the eddy-current problem of a jet entering a magnetic field (sec. 2.5).

In many ways mercury is an excellent candidate, but its vapor is toxic. Also, it may be preferable to use a material that is solid at room temperature, to simplify cleanup of spills. Lead alloys (solder-like materials) are good candidates. Rather low melting temperatures are obtained by alloying with indium, which, however, wets most solid metals so much as to make it difficult to produce liquid jets. Lead-bismuth alloys have the drawback of relatively high

Table 2: Properties of some candidate elements for primary targets.

Element	Z	Density (g/cm^3)	Melting Temp. (°C)	Boiling Temp. (°C)	Heat Cap. (J/g-°C)	Heat of Vapor. (J/g)	Thermal Cond. (W/cm-°C)	Resist. ($\mu\Omega$-cm)	Thermal Exp. (10^{-5}/°C)
Copper	29	8.96	1087	2567	0.39	4796	4.01	1.7	1.7
Zinc	30	7.1	420	906	0.39	1733	1.16	6.0	3.1
Gallium	31	5.9	30	2204	0.33	3712	0.4	26†	12
Indium	49	7.3	156	2073	0.23	2016	0.82	10	3.2
Tin	50	7.3	232	2270	0.18	2487	0.67	13	2.2
Mercury	80	13.6	−39	357	0.14	295	0.087	94†	6.1
Lead	82	11.35	327	1750	0.16	858	0.35	80†	2.9
Bismuth	83	9.7	271	1610	0.12	857	0.079	120	1.3

† liquid

production of polonium when activated by the proton beam. Gallium alloys are nontoxic and can be liquid at room temperature, so the resulting ease of handling indicates their use in the initial stages of the R&D program. The relatively low atomic number, low density and low resistivity of gallium is somewhat undesirable for use in the final target.

4.1 Mercury

Studies of materials issues for use of mercury as a proton target include refs. [40, 81, 82, 83]. The tensile strength of liquid mercury has been studied by Briggs [84].

4.2 Lead Alloys

A lead alloy of particular interest is eutectic lead-bismuth, 45% Pb by weight, with a melting point of 126°C (255°F). Other interesting low-melting allows of lead and/or bismuth are made by adding cadmium, indium or tin. Some quaternary and quinternary alloys have extremely low melting temperature, such as alloys 117 and 136 (designated by their melting temperatures in °F). Table 3 gives a summary of physical properties of several commercial lead alloys.

We have verified that the resistivities of liquid-lead alloys are very similar to those of the corresponding solid, as listed in Table 3 [22].

An extensive literature exists on materials-handling issues for applications of lead alloys at nuclear reactors [85, 86, 87, 88, 89, 90].

Table 3: Lead Alloy Specifications from Belmont Metals. See also `http://www.indium.com/fusiblealloys.html`

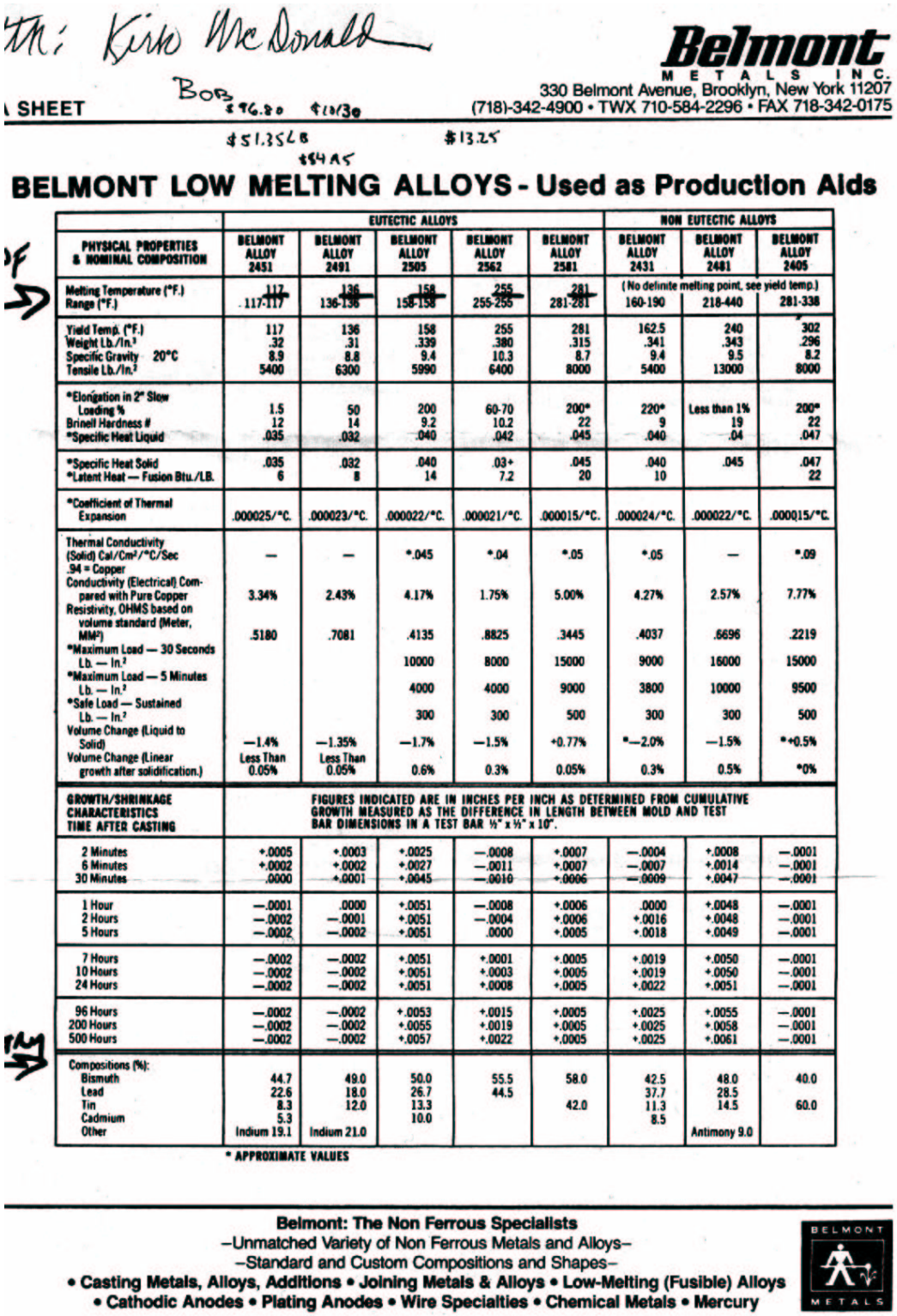

Attn: Kirk McDonald

Bob $76.80 $18/30

$51.3528 $13.25 $64.85

Belmont
METALS INC.
330 Belmont Avenue, Brooklyn, New York 11207
(718)-342-4900 • TWX 710-584-2296 • FAX 718-342-0175

SHEET

BELMONT LOW MELTING ALLOYS - Used as Production Aids

PHYSICAL PROPERTIES & NOMINAL COMPOSITION	EUTECTIC ALLOYS					NON EUTECTIC ALLOYS		
	BELMONT ALLOY 2451	BELMONT ALLOY 2491	BELMONT ALLOY 2505	BELMONT ALLOY 2562	BELMONT ALLOY 2581	BELMONT ALLOY 2431	BELMONT ALLOY 2481	BELMONT ALLOY 2405
Melting Temperature (°F.) Range (°F.)	~~117~~ 117-117	~~136~~ 136-136	~~158~~ 158-158	~~255~~ 255-255	~~281~~ 281-281	(No definite melting point, see yield temp.) 160-190	218-440	281-338
Yield Temp. (°F.)	117	136	158	255	281	162.5	240	302
Weight Lb./In.³	.32	.31	.339	.380	.315	.341	.343	.296
Specific Gravity 20°C	8.9	8.8	9.4	10.3	8.7	9.4	9.5	8.2
Tensile Lb./In.²	5400	6300	5990	6400	8000	5400	13000	8000
*Elongation in 2" Slow Loading %	1.5	50	200	60-70	200*	220*	Less than 1%	200*
Brinell Hardness #	12	14	9.2	10.2	22	9	19	22
*Specific Heat Liquid	.035	.032	.040	.042	.045	.040	.04	.047
*Specific Heat Solid	.035	.032	.040	.03+	.045	.040	.045	.047
*Latent Heat — Fusion Btu./LB.	6	8	14	7.2	20	10		22
*Coefficient of Thermal Expansion	.000025/°C.	.000023/°C.	.000022/°C.	.000021/°C.	.000015/°C.	.000024/°C.	.000022/°C.	.000015/°C.
Thermal Conductivity (Solid) Cal/Cm²/°C/Sec .94 = Copper	—	—	*.045	*.04	*.05	*.05	—	*.09
Conductivity (Electrical) Compared with Pure Copper	3.34%	2.43%	4.17%	1.75%	5.00%	4.27%	2.57%	7.77%
Resistivity, OHMS based on volume standard (Meter, MM²)	.5180	.7081	.4135	.8825	.3445	.4037	.6696	.2219
*Maximum Load — 30 Seconds Lb. — In.²			10000	8000	15000	9000	16000	15000
*Maximum Load — 5 Minutes Lb. — In.²			4000	4000	9000	3800	10000	9500
*Safe Load — Sustained Lb. — In.²			300	300	500	300	300	500
Volume Change (Liquid to Solid)	—1.4%	—1.35%	—1.7%	—1.5%	+0.77%	*—2.0%	—1.5%	*+0.5%
Volume Change (Linear growth after solidification.)	Less Than 0.05%	Less Than 0.05%	0.6%	0.3%	0.05%	0.3%	0.5%	*0%
GROWTH/SHRINKAGE CHARACTERISTICS TIME AFTER CASTING	FIGURES INDICATED ARE IN INCHES PER INCH AS DETERMINED FROM CUMULATIVE GROWTH MEASURED AS THE DIFFERENCE IN LENGTH BETWEEN MOLD AND TEST BAR DIMENSIONS IN A TEST BAR ½" x ½" x 10".							
2 Minutes	+.0005	+.0003	+.0025	—.0008	+.0007	—.0004	+.0008	—.0001
6 Minutes	+.0002	+.0002	+.0027	—.0011	+.0007	—.0007	+.0014	—.0001
30 Minutes	.0000	+.0001	+.0045	—.0010	+.0006	—.0009	+.0047	—.0001
1 Hour	—.0001	.0000	+.0051	—.0008	+.0006	.0000	+.0048	—.0001
2 Hours	—.0002	—.0001	+.0051	—.0004	+.0006	+.0016	+.0048	—.0001
5 Hours	—.0002	—.0002	+.0051	.0000	+.0005	+.0018	+.0049	—.0001
7 Hours	—.0002	—.0002	+.0051	+.0001	+.0005	+.0019	+.0050	—.0001
10 Hours	—.0002	—.0002	+.0051	+.0003	+.0005	+.0019	+.0050	—.0001
24 Hours	—.0002	—.0002	+.0051	+.0008	+.0005	+.0022	+.0051	—.0001
96 Hours	—.0002	—.0002	+.0053	+.0015	+.0005	+.0025	+.0055	—.0001
200 Hours	—.0002	—.0002	+.0055	+.0019	+.0005	+.0025	+.0058	—.0001
500 Hours	—.0002	—.0002	+.0057	+.0022	+.0005	+.0025	+.0061	—.0001
Compositions (%):								
Bismuth	44.7	49.0	50.0	55.5	58.0	42.5	48.0	40.0
Lead	22.6	18.0	26.7	44.5		37.7	28.5	
Tin	8.3	12.0	13.3		42.0	11.3	14.5	60.0
Cadmium	5.3		10.0			8.5		
Other	Indium 19.1	Indium 21.0					Antimony 9.0	

* APPROXIMATE VALUES

Belmont: The Non Ferrous Specialists
–Unmatched Variety of Non Ferrous Metals and Alloys–
–Standard and Custom Compositions and Shapes–
• Casting Metals, Alloys, Additions • Joining Metals & Alloys • Low-Melting (Fusible) Alloys
• Cathodic Anodes • Plating Anodes • Wire Specialties • Chemical Metals • Mercury

BELMONT METALS

4.3 Gallium and Gallium Alloys

Some information on liquid gallium alloys can be found at
`http://www.indium.com/liquidalloys.html`

The eutectic Ga-Sn alloy is particularly convenient, as it is a liquid at room temperature. It is easy to prepare by dissolving tin wire (but not powder) in liquid gallium at 40-50°C. The binary phase diagram for Ga-Sn is shown in Fig. 8.

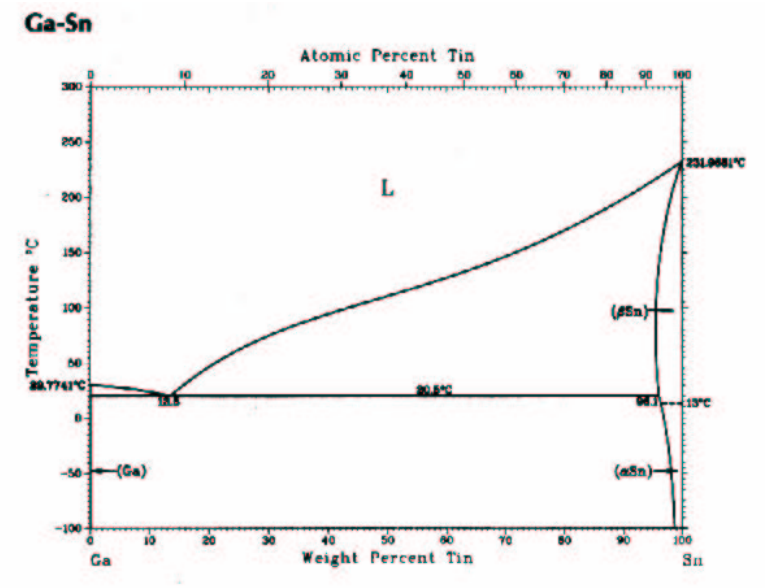

Figure 8: Ga-Sn phase diagram. Minimum melting temperature = 20.5°C [91].

Liquid gallium has a viscosity of 1.6 cp/g-cm^3, only slightly highly than that of water. The temperature dependence of the resistivity of gallium has been studied in detail [92]. Liquid gallium has been used as a coolant for silicon crystals at synchrotron light sources [93, 94].

4.4 Exotic Target Materials

The interaction of moving metals with the 20-T capture magnet (sec. 2.5) could be avoided by use of insulating liquids such as molten PtO_2 or Re_2O_3, or by granular materials such as slurries (*e.g.*, Pt in water) or powders [29].

The problem of beam-induced thermal shock (sec. 2.1.2) might be minimized by use of materials with very low (or negative) thermal expansion coefficients [19]. For example, Invar alloys have been studied for many years, and their properties are well known. Other materials are less well understood. For example, oxides such as ZrW_2O_8 produce a net contraction over a range of 1-1200°K. Bismuth ice slurries have the property, like water ice, of contracting when melting. Aqueous salt suspensions such as iron formate and sodium chloride contract with heating due to a molecular electrostrictive effect. Molecular liquids such as molten SiO_2 exhibit a negative thermal expansion in the region of 1700°C due to a molecular-bond modification.

Bubbly liquids may also have a higher compressibility, which would make them useful [40].

5 Jet Velocity

To be useful as a target, a pulsed liquid jet must have a minimum velocity, so that each pulse is sufficiently distinct from the others, and so that the jet is reasonably straight. The minimum velocity for a conductive jet to enter a strong magnetic field is considered in sec. 2.5.

5.1 Effect of 15-Hz Repetition Rate

We consider the use of a pulsed jet, leading to a series of cylinders of liquid, each of length l and radius r, and moving with velocity v. The frequency f of the pulse is nominally 15 Hz.

If the material from one pulse is not to overlap that of the next, then the jet velocity must obey

$$v > fl. \tag{5}$$

For example, if the length of each pulse is be about two nuclear interaction lengths (about 30 cm for a dense, high-Z material), then with $f = 15$ Hz, we need $v > 4.5$ m/s.

The jet velocity will have to be several times this to create gaps between adjacent pulses, so that the proton beam interacts with only a single jet pulse.

5.2 Effect of Gravity

The trajectory of the jet will be a parabolic arc, due to the acceleration of gravity. If the jet velocity were too low, the curvature of the jet would be large, and the proton beam would not be able to intersect the jet pulse over its whole length.

The ends of the jet are displaced downward from the ideal straight trajectory by amount

$$\Delta y = \frac{gt^2}{2} = \frac{gl^2}{8v^2}, \tag{6}$$

noting that the time for the center of the jet to reach its end is $t = l/2v$. For example, with $\Delta y = 1/8$ cm, as might be desired for a jet of radius 1 cm, $l = 30$ cm, we find $v \approx 1000$ cm/s $= 10$ m/s.

Thus, the effects of pulse frequency and of gravitational curvature both require the jet velocity to be at least 10 m/s.

5.3 Jet Velocity *vs.* Pressure

Suppose the liquid metal is stored in a tank of area A perpendicular to the flow, and the pressure is P above ambient. A valve lets a jet of liquid escape through an aperture of area $a \ll A$.

Then Bernoulli's equation tells us that the flow velocity v out the aperture obeys

$$\frac{1}{2}\rho v^2 = P + \frac{1}{2}\rho V^2, \tag{7}$$

where ρ is the density of the liquid and V is the velocity of the liquid surface of area A in the tank. The equation of continuity for an incompressible liquid tells us that $av = AV$, so that

$$v = \sqrt{\frac{2P}{\rho(1-(a/A)^2)}} \approx \sqrt{\frac{2P}{\rho}}. \tag{8}$$

For example, for merucyr of density $\rho \approx 13.6$ g/cm^3,

$$v[\text{m/s}] \approx \sqrt{15P[\text{atm.}]}. \tag{9}$$

Thus, to reach $v = 4.5$ m/s would require 1.4 atm overpressure in the storage tank; 27 atm would be required to reach a velocity of 20 m/s.

6 The Interaction of a Liquid-Metal Jet with a Magnetic Field

As a jet of liquid metal enters the magnetic field that surrounds the beam interaction region, it will be repelled according to Lenz' law. The effect is due to the Lorentz force on the eddy currents induced in the moving metal. In an extreme case the jet would not reach the center of the interaction region.

Here we present simplified analytic estimates of the effects of eddy currents, and reach the tentative conclusion that they would visibly alter the trajectory of the liquid-metal jet, but would not prevent the jet from functioning as a target. However, there appears to be little safety margin, suggesting the need for laboratory experiments to confirm that the proposed liquid-metal jet is viable.

Additional details of the analytic arguments can be found in refs. [20, 21, 22, 23, 24, 25, 26, 27, 28].

It is useful to establish numerical values for some relevant parameters of our system as a qualitative guide to its magnetohydrodynamic behavior.

First, we note that the problem of a moving conductor in a static magnetic field is equivalent to a moving field that encounters a conductor initially at rest. Thus, the electric field $\mathbf{E}'$ in the frame of the conductor is related to the electric and magnetic fields $\mathbf{E}$ and $\mathbf{B}$ in the lab frame by

$$\mathbf{E}' = \mathbf{E} + \mathbf{v} \times \mathbf{B}, \tag{10}$$

where $\mathbf{v}$ is the laboratory velocity of the conductor ($v \ll c$), and we use MKSA units.

Next, we recall that the penetration of a time-dependent magnetic field into a conductor is governed by a diffusion equation. Assuming $v \ll c$ and reasonably good conductivity σ, we may neglect the displacement current, and the basic electromagnetic equations are

$$\nabla \times \mathbf{E} = -\frac{\partial \mathbf{B}}{\partial t}, \qquad \nabla \times \mathbf{B} = \mu_0 \mathbf{j}, \qquad \text{and} \qquad \mathbf{j} = \sigma \mathbf{E}' = \sigma(\mathbf{E} + \mathbf{v} \times \mathbf{B}), \tag{11}$$

where $\mathbf{j}$ is the current density. On eliminating $\mathbf{j}$ and $\mathbf{E}$ we find that

$$\frac{\partial \mathbf{B}}{\partial t} = \frac{\nabla^2 \mathbf{B}}{\mu_0 \sigma} + \nabla \times (\mathbf{v} \times \mathbf{B}). \tag{12}$$

With the neglect of the second term (justified for low velocity), we find the desired diffusion equation. Thus, the characteristic time for diffusion of the magnetic field into a long conducting cylinder of radius r is

$$\tau = \mu_0 \sigma r^2. \tag{13}$$

The low-melting temperature alloys in Table 3 all have relatively low conductivity. In particular, alloy 255 has conductivity only 2% that of copper (resistivity = 1.67 $\mu\Omega$-cm), *i.e.*, about 10^6 MKSA units. Mercury also has conductivity close to 10^6 MKSA units. Hence, for a cylinder of radius 1 cm of a candidate liquid metal, the diffusion time is

$$\tau \approx 4\pi \times 10^{-7} \cdot 10^6 (10^{-2})^2 \approx 10^{-4} \text{ sec.} \tag{14}$$

Another characteristic time in our problem is that over which the external magnetic field varies appreciably, from the point of view of the liquid jet. For a jet of velocity v that enters a solenoid of diameter D, this time is D/v. The ratio of the diffusion time to time D/v is called the magnetic Reynold's number:

$$\mathcal{R} = \frac{\tau v}{D}. \tag{15}$$

For $\mathcal{R} \ll 1$ the external magnetic field penetrates the conductor, but for $\mathcal{R} \gg 1$ it does not.

Anticipating a jet velocity of order 20 m/s and a solenoid of diameter $D \approx 0.2$ m, we have $D/v \approx 0.1$ s, and the magnetic Reynold's number is $\mathcal{R} \approx 0.01$. We conclude that in our problem the diffusion is rapid enough that the external field penetrates the conductor. That is, our candidate metals are not sufficiently "good" conductors to exclude the magnetic field from their interior. This is fortunate, as a "good" conductor could not enter a 20-T magnetic field unless its initial velocity were very high.[1]

The magnetic Reynold's number can be thought of in another way. From the point of view of the conductor, the external magnetic field is time dependent with frequency content up to $\omega \approx v/D$. The skin depth at this frequency is $\delta = \sqrt{2/\mu_0 \omega \sigma} = \sqrt{2D/\mu_0 \sigma v}$. This is to be compared to the radius r of the conductor. Indeed,

$$\frac{r^2}{\delta^2} = \frac{\mu_0 \sigma r^2 v}{2D} = \frac{\mathcal{R}}{2}. \tag{16}$$

In our case, the low value of the magnetic Reynold's number indicates that the conductor is much smaller than the relevant skin depth, and again we expect the external field to penetrate the conductor.

We now give some approximate analyses of the forces on the liquid jet as it enters a solenoid.

[1]To see this, consider a good conductor moving along the z-axis of a solenoid field. Surface current $I = B_z/\mu_0$ (per unit length) is induced so as to cancel the external solenoid field B_z. This current interacts with the radial component of the external field, $B_r \approx -(r/2)dB_z(0,z)/dz = -rB_z'/2$ to produce retarding force $F = -2\pi r I B_r = -2\pi r (B_z/\mu_0)(rB_z'/2) = \pi r^2 (B_z^2)'/2\mu_0$ per unit length. But also, $F = ma = \pi r^2 \rho \dot{v} = \pi r^2 \rho v v' = \pi r^2 \rho (v^2)'/2$, where $\rho \approx 10^4$ kg/m^3 is the mass density. This integrates to give $v^2(z) = v_{-\infty}^2 - B_z^2/\mu_0 \rho$. Thus, to enter a field of $B_z = 20$T, the initial velocity would need to be at least $B_z/\sqrt{\mu_0 \rho} \approx 200$ m/s for our heavy metals.

6.1 Jet on Axis of a Solenoid

We model the forces on a conducting jet in a magnetic field by considering only a ring (or disc) perpendicular to the axis of the jet. The ring has radius r, radial extent Δr and thickness Δz.

We first consider only motion along the axis of the ring, which we call the z axis, and which is also the axis of a solenoid magnet with field $\mathbf{B}(r, z)$.

Then the magnetic flux through the ring at position z is

$$\Phi \approx \pi r^2 B_z(0, z), \tag{17}$$

whose time rate of change is

$$\dot{\Phi} = \pi r^2 \dot{B}_z = \pi r^2 B_z' v, \tag{18}$$

where $\dot{}$ indicates differentiation with respect to time, $'$ is differentiation with respect to z, B_z stands for $B_z(0, z)$, and v is the velocity of the center of mass of the ring.

If the metal has electrical conductivity σ, then its resistance to currents around the ring is

$$R = \frac{2\pi r}{\sigma \Delta r \Delta z}, \tag{19}$$

so the (absolute value of the) induced current is

$$I = \frac{\mathcal{E}}{R} = \frac{\dot{\Phi}}{R} = \frac{\sigma r B_z' v \Delta r \Delta z}{2}. \tag{20}$$

6.1.1 Radial Pinch.

The Lorentz force on the ring due to the interaction of this current with the axial field pinches the jet radially, while that due to the interaction with the radial field opposes the motion. The radial pinch can be characterized by a radial pressure gradient,

$$\frac{\Delta P_r}{\Delta r} = \frac{\Delta F_r}{\Delta r \Delta z \Delta l} = -\frac{B_z I \Delta l}{\Delta r \Delta z \Delta l} = -\frac{\sigma r B_z B_z' v}{2}. \tag{21}$$

As the jet enters the magnet from $z = -\infty$, the axial field gradient, B_z', is initially positive, and the radial forces are inward. However, as the jet exits the solenoid, the gradient B_z' becomes negative, and the radial force is outwards. Even if the jet has not been destabilized by the pinch on entering the magnetic, the radially outward forces experienced on leaving the magnet may disperse the jet.

The pinch is greatest as the ring passes the edge of the solenoid, where $B_z \approx B_0/2$ and $B_z' \approx B_0/D$ for a solenoid of diameter D and peak axial field B_0. That is,

$$\frac{\Delta P_{r,\max}}{\Delta r} \approx -\frac{\sigma}{4}\frac{r}{D} B_0^2 v. \tag{22}$$

Integrating this over radius, the pressure gradient between the axis and radius r is

$$\Delta P_{r,\max} \approx -\frac{\sigma}{8}\frac{r^2}{D} B_0^2 v. \tag{23}$$

In general, the pinch will cause the jet to shrink radially and elongate axially. Instabilities in this process may break the jet up into droplets. However, once the jet begins to deform, additional eddy currents are induced that will oppose the deformation. See sec. 2.5.2.

As a very crude model of the effect of the pinch on the radius of the jet, we suppose that the jet surface accelerates inwards during the characteristic time D/v under a force approximated by the pinch pressure $\Delta P_{r,\max}$ times the surface area. Then eq. (23) leads to the estimate

$$\Delta r \approx -\frac{\sigma}{16}\frac{rD}{\rho v}B_0^2 \tag{24}$$

for the radial perturbation caused by the pinch.

6.1.2 Axial Retarding Force.

The component of the Lorentz force that opposes the motion of the ring is

$$\Delta F_z = 2\pi r B_r I = -\pi\sigma r^2 B_r B_z' v \Delta r \Delta z \approx -\frac{\pi\sigma r^3 (B_z')^2 v \Delta r \Delta z}{2}, \tag{25}$$

using the approximate relation for the radial field near the z-axis,

$$B_r(r,z) \approx -\frac{r}{2}\frac{dB_z(0,z)}{dz} = -\frac{rB_z'}{2}, \tag{26}$$

as can be deduced from the Maxwell equation $\nabla \cdot \mathbf{B} = 0$.

The equation of motion of a ring is then

$$dF_z = -\frac{\pi\sigma r^3 (B_z')^2 v_z \Delta r \Delta z}{2} = m\dot{v}_z = 2\pi\rho r \Delta r \Delta z v_z' v_z, \tag{27}$$

where ρ is the mass density of the metal. After dividing out the common factor of $\pi r \Delta r \Delta z v_z$ we find

$$v_z'(r) = -\frac{\sigma r^2 (B_z')^2}{4\rho}. \tag{28}$$

Before considering a detailed model of the axial field profile, B_z, we note that the peak gradient of the axial field of a solenoid of diameter D is B_0/D, and the gradient is significant over a region $\Delta z \approx D$. Hence, we estimate that on entering a solenoid the jet velocity is reduced by an increment

$$\Delta v_z(r) \approx \frac{\sigma r^2 B_0^2}{4\rho D}. \tag{29}$$

On leaving the solenoid, the jet velocity is reduced by a second increment Δv_z. (Since the effect depends on $(B_z')^2$, the force is retarding on both entering and exiting, as predicted by Lenz' law.)

The jet velocity cannot actually go negative whatever the magnetic field . If the velocity reaches zero, the jet stops (falls). Note that we divided eq. (27) by v_z before integrating; once v_z becomes zero, F goes to zero and stays there.

The reduction of velocity (29) is zero on the axis of the jet, and grows quadratically with radius. If the jet were a rigid body, Δv_z would be one half the value given by eq. (29) at the outer radius.

If the change in velocity is small compared to the initial velocity, $v_{-\infty}$, we estimate the distance $\Delta z(r)$ by which the material in the jet at radius r is retarded compared to the material on axis as

$$\Delta z(r) \approx \Delta v_z(r) \Delta t \approx \Delta v_z(r) \frac{D}{v_{-\infty}} \approx \frac{\sigma r^2 B_0^2}{4\rho v_{-\infty}}. \tag{30}$$

We desire this to be small compared to the length of the jet. Indeed, it will be awkward if Δ_z exceeds the radius of the jet.

We now consider a more specific model. See [22] for discussion of a finite solenoid.

6.1.3 Semi-Infinite Solenoid.

The field on the axis of a semi-infinite solenoid is amenable to analytic calculation. Indeed, for a solenoid of radius $D/2$ with windings from $z = 0$ to $+\infty$, the axial field is

$$B_z(0, z) = \frac{B_0}{2} \left(1 + \frac{z}{\sqrt{(D/2)^2 + z^2}} \right), \tag{31}$$

whose derivative is

$$B_z' = \frac{dB_z(0, z)}{dz} = \frac{B_0}{2} \frac{(D/2)^2}{[(D/2)^2 + z^2]^{3/2}}. \tag{32}$$

Using eq. (32) in eq. (28) and integrating the equation of motion from $-\infty$ to z, we find

$$v_z(r, z) = v_{-\infty} - \frac{3\sigma r^2 B_0^2}{64\rho D} \left(\frac{\pi}{2} + \tan^{-1} w + \frac{w}{1 + w^2} + \frac{2w}{3(1 + w^2)^2} \right), \tag{33}$$

where D is the diameter of the solenoid and $w = 2z/D$.

The semi-infinite solenoid is meant to approximate a finite solenoid of length $L = \alpha D$. Since the semi-infinite coil begins at $z = 0$, the center of the finite solenoid it approximates is at $z = \alpha D/2$, *i.e.*, at $w = \alpha$. For $\alpha \gtrsim 1$, as is reasonable for an actual magnet, there is little difference between the result of eq. (33) at $w = \alpha$ and at $+\infty$, so we estimate the change in velocity as

$$\Delta v_z(r) \approx -\frac{3\pi\sigma r^2 B_0^2}{64\rho D}. \tag{34}$$

The retardation relative to the center of the jet is related by

$$\Delta \dot{z}(r) = \Delta v_z(r) = \Delta z' v_z \approx \Delta z' v_{-\infty}, \tag{35}$$

where the approximation holds if $\Delta v_z \ll v_{-\infty}$. In this approximation, we integrate eq. (33) to find

$$\Delta z(r) \approx -\frac{3\sigma r^2 B_0^2 w}{128\rho v_{-\infty}} \left(\frac{\pi}{2} + \tan^{-1} w - \frac{1}{3w(1 + w^2)} \right). \tag{36}$$

This diverges for large w, but at $w = \alpha \approx 1$, corresponding to the center of a real magnet, we have

$$\Delta z(r) \approx -\frac{3\pi\sigma r^2 B_0^2 \alpha}{128\rho v_{-\infty}}. \tag{37}$$

6.1.4 Numerical Examples.

We consider the lead-bismuth alloy 255, whose conductivity is about 10^6 MKSA units and whose density is about 10 gm/cm^3, *i.e.*, 10^4 kg/m^3. Then, eq. (34) leads to the requirement

$$v_{-\infty} > 60 \text{ m/s} \left[\frac{r}{1 \text{ cm}}\right] \left[\frac{r}{D}\right] \left[\frac{B_0}{20 \text{ T}}\right]^2 . \tag{38}$$

It is thought that the jet radius must be 0.5-1 cm to match the proton beam, and that the inside diameter of the solenoid will be about 20 cm. In this case we need $v_{-\infty} > 0.75$-3 m/s for $B_0 = 20$ T.

Again, if the jet is to exit the magnet, $v_{-\infty}$ must be twice the minimum given in (38).

In the approximation of eq. (37), the shear in the jet profile between its axis and radius r is

$$\frac{\Delta z(r)}{r} \approx -3\alpha \left[\frac{r}{1 \text{ cm}}\right] \left[\frac{B_0}{20 \text{ T}}\right]^2 \left[\frac{10 \text{ m/s}}{v_{-\infty}}\right] . \tag{39}$$

For, say, $r = 1$ cm, $v_{-\infty} = 10$ m/s, $\alpha = 2$ and $B_0 = 20$ T, we would have $\Delta z(r) \approx 6r$, which is a fairly severe distortion of the jet.

Returning to the issue of the radial pinch, we can now cast eq. (23) in the form

$$\Delta P_{r,\max} \approx 50 \text{ atm} \left[\frac{r}{1 \text{ cm}}\right] \left[\frac{r}{D}\right] \left[\frac{B_0}{20 \text{ T}}\right]^2 \left[\frac{v_{-\infty}}{10 \text{ m/s}}\right] . \tag{40}$$

For, say, $r = 1$ cm, $v_{-\infty} = 10$ m/s, $D = 20$ cm and $B_0 = 20$ T, the maximum radial pressure is 2.5 atmospheres. This may be enough to perturb the shape of the jet as it enters the magnet.

When the jet leaves the magnet, the radial pressure goes negative. This pressure is small compared to the tensile strength of the jet material, so the jet will not necessarily tear apart. However, the rapid change of pressure from positive to negative may excite oscillations of the jet which lead to breakup into macroscopic droplets. This would occur after the proton beam interacted with the jet, so is more of a nuisance for the liquid-collection system than a fundamental flaw.

The longitudinal effects, (38) and (39), are suppressed at higher jet velocities, which, however, enhance the radial pinch (40).

6.2 Magnetic Damping of Radial Perturbations

If the liquid jet deforms, either due to the Lorentz forces on the eddy currents or due to the beam-induced pressure wave that was discussed in sec. 2.1.2, further eddy currents will arise, leading to further Lorentz forces that damp the deformation.

To estimate this, we follow the argument of sec. 2.5.1 for a conducting ring of radius r perpendicular to a magnetic field B_0. Suppose the ring is being deformed with a radial velocity v_r, either inwards or outwards. Then the rate of change of magnetic flux through the ring is $\dot{\Phi} = 2\pi r v_r B_0$, and the eddy current induced in a ring of cross section $\Delta r \Delta z$ is $I = \sigma \Delta r \Delta z v_r B_0$, where σ is the conductivity. The Lorentz force on this current leads to a radial pressure gradient of magnitude

$$\frac{\Delta P_r}{\Delta r} = \frac{\Delta F_r}{\Delta r \Delta z \Delta l} = \frac{B_0 I \Delta l}{\Delta r \Delta z \Delta l} = \sigma v_r B_0^2 . \tag{41}$$

The total damping pressure at radius r is therefore

$$\Delta P_{r,\mathrm{damp}} \approx \sigma r v_r B_0^2. \tag{42}$$

As a first example, consider inward radial motion caused by the pinch pressure (23). In the first approximation, the jet surface accelerates inwards during the characteristic time D/v_z under a force approximated by the pinch pressure $\Delta P_{r,\max}$ times the surface area. Then eq. (23) leads to the estimate for the radial velocity:

$$v_r \approx -\frac{\sigma}{4}\frac{r}{\rho}B_0^2. \tag{43}$$

Combining this with eq. (42), the damping pressure is

$$\Delta P_{r,\mathrm{damp}} \approx \frac{\sigma^2 r^2 B_0^4}{4\rho}. \tag{44}$$

For a liquid-metal jet of conductivity 10^6 MKSA, radius 1 cm, and inside a 20-T field, the damping pressure is about 4,000 atm. This greatly exceeds the pinch pressure of 2.5 atm estimated above, and suggests that the radial motion due to the pinch is highly damped.

As a second example, consider the same jet that is now being blown apart with a radial velocity $v_r = 1,000$ m/s by the beam-induced shock. Then the damping pressure (42) is 4 GPa, which equals the tensile strength of steel, and so might hold the jet together.

The damping pressure in the second example is about 20 times the magnetic pressure, $B_0^2/2\mu_0$.

Thus, it is encouraging that significant damping of all radial perturbations will occur in a strong magnetic field.

6.3 Jet at an Angle to the Axis of a Solenoid

To improve the yield of pions in the interaction of the proton beam with the liquid jet, it is desirable that the jet axis make a small angle $\theta \approx 0.1$ to the axis of the solenoid. In this case the motion of the jet includes a component perpendicular to the magnetic field.

The induced eddy currents will flow in loops that are roughly perpendicular to the magnetic field lines. As a simplification, we suppose that the current loops are circles perpendicular to the axis of the solenoid. This approximation should be reasonable for small θ.

The (unperturbed) trajectory of the conductor of radius a is taken to be along the line

$$x = z\theta, \tag{45}$$

where z increases with increasing time. To simplify the calculations, we suppose the trajectory follows eq. (45), even though the velocity of the jet is perturbed by the magnetic field (impulse approximation).

Following the same line of argument as in sec. 2.5.1 we again calculate the drag force induced on the conducting disc. The force element on a piece of the disk at radius $r = \epsilon a$ and azimuth ϕ is found to be [22]

$$\begin{aligned} d\mathbf{F} &= Id\mathbf{l} \times \mathbf{B} \qquad (46)\\ &= I\epsilon a d\phi \left[(\hat{\mathbf{x}}\cos\phi + \hat{\mathbf{y}}\sin\phi)\left(B_z - \frac{(z\theta)^2 + (\epsilon a)^2 + 2\epsilon a z\theta\cos\phi}{4} B_z'' \right) + \hat{\mathbf{z}}\frac{B_z'}{2}(\epsilon a + z\theta\cos\phi) \right], \end{aligned}$$

where $\hat{\rho}$ is the unit vector pointing radially outwards from the axis of the jet ($\rho = \epsilon a$).

The transverse force can be decomposed into a radial pinch (or expansion) as discussed in sec. 2.5.1 plus a drag in the x direction. The longitudinal (z) force vanishes on the axis of the jet, has a drag that is independent of azimuth, and another component that varies with azimuth, causing a torque (or shear).

6.3.1 Drag Forces.

We first ignore the radial pinch and the shear by integrating eq. (46) over ϕ and using eq. (20) for I to obtain

$$d\mathbf{F} = \frac{\pi\sigma a^4 v_z B_z' \epsilon^3 \Delta\epsilon \Delta z}{2}\left(\hat{\mathbf{x}}\frac{z\theta B_z''}{2} - \hat{\mathbf{z}}B_z'\right). \tag{47}$$

The z component of the drag force is the same as found previously in eq. (25). The retarding force vanishes on the jet axis, and increases as the cube of the radius within the jet. As a result, the core of the jet will move ahead of the outer regions.

In turn, we integrate (47) over ϵ to obtain the total force on a disc of thickness Δz:

$$\mathbf{F} = \frac{\pi\sigma a^4 v_z B_z' \Delta z}{8}\left(\hat{\mathbf{x}}\frac{z\theta B_z''}{2} - \hat{\mathbf{z}}B_z'\right). \tag{48}$$

In the equation of motion, we again replace differentiation by time with that by z:

$$\mathbf{F} = m\dot{\mathbf{v}} = \pi a^2 \Delta z \rho v_z \mathbf{v}'. \tag{49}$$

The components of the equation of motion of the conducting jet are thus,

$$v_x' = \frac{\sigma a^2 z\theta B_z' B_z''}{16\rho}, \qquad \text{and} \qquad v_z' = -\frac{\sigma a^2 (B_z')^2}{8\rho}. \tag{50}$$

We use the example of a semi-infinite solenoid to illustrate the effect of the eddy currents on the jet velocity, because the needed field derivatives have simple analytic forms. The form of the trajectory, (45), assumes that the center of the magnet is at the origin. Suppose the length of the physical magnet is α times its diameter D, so that the coil extends over $-\alpha D/2 \le z \le \alpha D/2$. Then the field of the physical magnet can be represented by the field of a semi-infinite solenoid beginning at $z = -\alpha D/2$.

From the derivatives of eq. (31) we see that v_z' is always negative, but that v_x' is negative only until the jet enters the magnet ($z = -\alpha D/2$). Integrating (50) from $-\infty$ to z, we find that the velocity components of the jet are

$$v_x = v_{x,-\infty} - \frac{3\sigma a^2 B_0^2 \theta}{1024\rho D}\left[\frac{\pi}{2} + \tan^{-1} w + \frac{w}{1+w^2} + \frac{2w}{3(1+w^2)^2} - \frac{16z}{3D(1+w^2)^3}\right], \tag{51}$$

and

$$v_z = v_{z,-\infty} - \frac{3\sigma a^2 B_0^2}{128\rho D}\left[\frac{\pi}{2} + \tan^{-1} w + \frac{w}{1+w^2} + \frac{2w}{3(1+w^2)^2}\right], \tag{52}$$

where $w = 2z/D + \alpha$. Of course, $v_{x,-\infty} = \theta v_{z,-\infty}$ by assumption. The velocity components of the jet when it reaches the center of the magnet ($z = 0,\ w = \alpha$) are

$$v_{x,0} = \theta v_{z,-\infty} - \frac{3\sigma a^2 B_0^2 \theta}{1024 \rho D}\left[\frac{\pi}{2} + \tan^{-1}\alpha + \frac{\alpha}{1+\alpha^2} + \frac{2\alpha}{3(1+\alpha^2)^2}\right], \tag{53}$$

and

$$v_{z,0} = v_{z,-\infty} - \frac{3\sigma a^2 B_0^2}{128 \rho D}\left[\frac{\pi}{2} + \tan^{-1}\alpha + \frac{\alpha}{1+\alpha^2} + \frac{2\alpha}{3(1+\alpha^2)^2}\right], \tag{54}$$

Thus, while both v_x and v_z are reduced on entering the solenoid, the relative reduction in the x velocity is only 1/8 that of the z velocity. As a consequence, the angle θ of the trajectory to the axis of the solenoid actually increases as the jet enters the magnet. For example, suppose that $v_{z,-\infty}$ is 3 times the loss of velocity on entering the magnet. Then

$$v_{z,0} = \frac{2}{3} v_{z,-\infty}, \qquad v_{x,0} = \frac{23}{24}\theta v_{z,-\infty}, \tag{55}$$

and the angle of the trajectory at the center of the magnet is

$$\theta_0 = \frac{v_{x,0}}{v_{z,0}} = \frac{69}{48}\theta = 1.44\theta. \tag{56}$$

Figure 9 illustrates the variation of v_x, v_z and θ of the jet as a function of z.

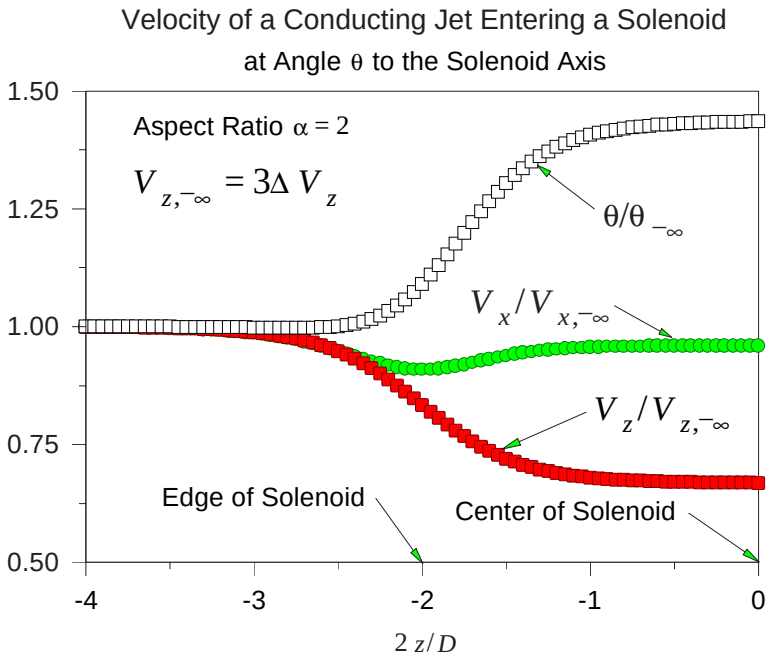

Figure 9: v_x, v_z and θ of the jet as a function of z as it enters a solenoid of aspect ratio $\alpha = 2$, according to eqs. (51-52). The initial z velocity of the jet is taken to be 3 times the loss of velocity on entering the solenoid.

We are greatly encouraged by these idealized calculations that the effect of eddy currents on the transverse velocity of the jet will not be too severe.

The above analysis is for the drag force on the jet as a whole. Recall that the force varies with radius within the jet, and so leads to longitudinal distortions as discussed in sec. 2.5.1. The variation of the drag force in x leads to additional torques and shears, which we now discuss.

6.3.2 Torque and Shear.

The magnetic forces on the eddy currents also produce a torque that will twist the jet about the axis perpendicular to the plane of the jet motion, the y axis in our example.

The torque $d\mathbf{N}$ on a small element of a current ring about its center can be calculated from eq. (46). On integrating over ϕ and ϵ we find that $N_x = 0$, and the total torque on a disc of radius a and thickness Δz is

$$N_y = \frac{\pi}{16} z\theta\sigma a^4 v_z B_z'^2 \Delta z \approx -\frac{xF_z}{2}. \tag{57}$$

The sense of rotation is opposite to that of the deflection of the jet trajectory as it enters the magnetic field.

The moment of inertia of the disc about a diameter is $ma^2/4 = \pi\rho a^4\Delta z/4$. Hence the angular acceleration of the azimuthal angle φ of the disc about the y axis is

$$\ddot{\varphi} = v_z \frac{d\dot{\varphi}}{dz} = \frac{\theta\sigma z B_z'^2 v_z}{4\rho}. \tag{58}$$

Note that this is independent of the radius of the jet. Using B_z' from eq. (31), we have

$$\frac{d\dot{\varphi}}{dz} = \frac{\theta\sigma B_0^2}{4\rho D^2} \frac{z}{(1+w^2)^3}, \tag{59}$$

where, as before, $w = 2z/D + \alpha$, and $\alpha = L/D$. This can be integrated once to give

$$\dot{\varphi} = v_z \frac{d\varphi}{dz} = -\frac{3\theta\sigma B_0^2}{128\rho} \left[\frac{\alpha\pi}{2} + \alpha \tan^{-1} w + \frac{\alpha w}{1+w^2} + \frac{2(1+\alpha w)}{3(1+w^2)^2} \right]. \tag{60}$$

If we ignore the variation in v_z with position, this can be integrated once more to yield

$$\varphi(z) = -\frac{3\theta\sigma B_0^2 D}{256\rho v_z} \left[\left(\alpha w + \frac{1}{3} \right) \left(\frac{\pi}{2} + \tan^{-1} w \right) + \frac{\alpha - w}{3(1+w^2)} \right]. \tag{61}$$

At the center of the magnet, $w = \alpha$, the total angle of rotation of the disc is

$$\varphi_{\text{center}} = -\frac{3\theta\sigma B_0^2 D}{256\rho v_z} \left[\left(\alpha^2 + \frac{1}{3} \right) \left(\frac{\pi}{2} + \tan^{-1} \alpha \right) \right] \approx -\frac{3\pi\alpha^2\theta\sigma B_0^2 D}{256\rho v_z}, \tag{62}$$

where the approximation holds for α somewhat larger than 1. For example, if $\alpha = L/D = 2$, $D = 0.2$ m, $B_0 = 20$ T and $v_z = 10$ m/s, we find $\varphi_{\text{center}} \approx -4\pi\theta$. With $\theta = 0.1$ rad, then $\varphi_{\text{center}} \approx -0.4\pi$.

Equation (60) indicates the interesting result that the rate of change of rotation is independent of the velocity, so the total rotation can be suppressed by increasing the jet velocity, thereby lowering the transit time.

A liquid jet would presumably not rotate as a rigid body. Rather, there would be a shear in which v_z of that portion of the jet closer to the magnet axis actually increases, while v_z decreases for material farther away (and by a larger absolute amount). Our estimate that $\varphi_{\text{center}} \approx 90^\circ$ can perhaps be reinterpreted as indicating that the shear distance along the jet axis will amount to roughly the jet radius when the jet reaches the center of the magnet. This would not be troublesome.

6.4 The Rayleigh Instability of the Jet

6.4.1 Zero Magnetic Field.

Following earlier work by Plateau, Rayleigh deduced that a cylindrical jet is unstable against perturbations of wavelength (along the jet axis) greater than the circumference of the jet [95]. The result of the instability is the breakup of the jet into droplets, commonly seen as water exits a nozzle. The characteristic time for onset of the instability is

$$\tau = 3\sqrt{\frac{r^3\rho}{T}}, \tag{63}$$

where the jet has radius r, mass density ρ and surface tension T. The distance travelled by a jet before breakup is then $v\tau$, where v is the jet velocity.

An example of breakup of a 0.5-mm-diameter mercury jet is shown in Fig. 10 [65, 66, 67]. The density of mercury is $\rho = 13.5$ g/cm^3, and the surface tension is $T = 470$ dyne/cm. Then eq. (63) gives $\tau = 0.002$ s for $r = 0.025$ cm. At 40 psi, the jet velocity was $v = 5$ m/s, so the characteristic length before breakup is predicted to be 1 cm, in good agreement with the reported value of 1.4 cm. It thus appears that Rayleigh's formula is valid for liquid-metal jets.

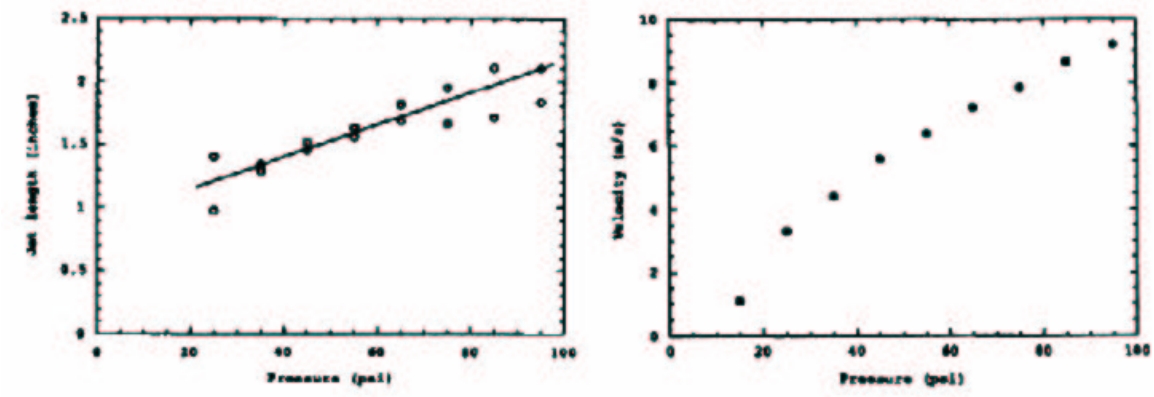

Figure 10: Length before breakup, and velocity of a mercury jet of radius 0.025 cm.

Turning to parameters relevant to the muon-collider target, consider a gallium jet of radius 1 cm. The density is $\rho = 6$ g/cm^2, and the surface tension is $T = 360$ dyne/cm. Then the instability time is $\tau = 0.4$ s. For a jet velocity of 10 m/s, the breakup length would be about 4 m, which is satisfactory. If the jet radius is reduced to 0.5 cm, the breakup length drops to 1.4 m.

6.4.2 Nonzero Axial Magnetic Field.

The effect of a uniform axial magnetic field on the Rayleigh instability has been considered by Chandrasekhar [96]. There is no change in the instability time for a nonconducting liquid, unless its permeability is significantly greater than one. For a conducting liquid, Chandrasekhar introduces a quality factor,

$$Q = \frac{\mu B^2}{4\pi\eta}\sqrt{\frac{r^3}{\rho T}}, \tag{64}$$

where μ is the permeability, B is the axial magnetic field strength, and η is called the "resistivity" ($\eta = c^2/4\pi\sigma$, where σ is the electrical conductivity). For $Q > 20$, the Rayleigh instability is suppressed in the first approximation.

For mercury, $\eta = 7.5 \times 10^3$ cm^2/s, and $Q = 1.33 \times 10^{-7} B^2 r^{3/2}$ in Gaussian units. Thus for a 20-T axial magnetic field and $r = 1$ cm, $Q \approx 5000$, and the Rayleigh instability should be almost completely damped. This conclusion is little changed by variations in the radius or resistivity by factors of 2, and should be valid for all liquid-metal jets under consideration here.

The quality factor does not drop to 20 until the field has fallen to slightly over 1 T (for $r = 1$ cm). Hence, unless the jet travels more than a meter in a region where the magnetic field is less than 1 T, the Rayleigh instability will be of little concern for us.

7 References

[1] J. Alessi *et al.*, *An R&D Program for Targetry and Capture at a Muon Collider Source* (Sept. 30, 1998, approved as BNL E951), sec. 2.5
http://www.hep.princeton.edu/~mcdonald/mumu/target/targetprop.pdf

[2] The $\mu^+\mu^-$ Collider Collaboration, *$\mu^+\mu^-$ Collider Feasibility Study*, BNL-52503, FERMILAB-Conf-96/092, LBNL-38946 (July 1996);
http://www.cap.bnl.gov/mumu/book.html

[3] C.M. Ankenbrandt *et al.*, *Status of muon collider research and development and future plans*, Phys. Rev. ST Accel. Beams **2**, 081001 (1999), http://prst-ab.aps.org/przv02i08tc.html
http://www.cap.bnl.gov/mumu/status_report.html

[4] N. Holtkamp and D. Finley, eds., *A Feasibility Study of a Neutrino Source Based on a Muon Storage Ring* (March 31, 2000),
http://www.fnal.gov/projects/muon_collider/nu-factory/nu-factory.html

[5] *The Neutrino Factory and Muon Collider Feasibility Study II*, http://www.cap.bnl.gov/mumu/studyii/

[6] N.V. Mokhov R. Noble and A. Van Ginneken, *Target and Collection Optimization for Muon Colliders*, AIP Conf. Proc. **372**, 61 (1996); http://www-lib.fnal.gov/archive/1996/conf/Conf-96-006.html

[7] D. Ehst, N.V. Mokhov, R.J. Noble and A. Van Ginneken, *Target Options and Yields for a Muon Collider Source*, Proc. PAC97 (Vancouver, 1997), p. 393; http://www.triumf.ca/pac97/papers/pdf/4W023.PDF

[8] H. Takahashi, Y. An, X. Chen and M. Nomura, *Optimization of the Target for Muon Colliders*, Proc. PAC97 (Vancouver, 1997), p. 402; http://www.triumf.ca/pac97/papers/pdf/4W027.PDF

[9] N.V. Mokhov and A. Van Ginneken, *Pion Production and Targetry at $\mu^+\mu^-$ Colliders*, AIP Conf. Proc. **441**, 320 (1998); http://www-ap.fnal.gov/~mokhov/papers/1998/Fermilab-Conf-98-41.ps

[10] S.H. Kahana, Y. Pang and T.J. Schlagel, in *Proceedings of Heavy Ion Physics at the AGS-HIPAGS '93*, eds. G.S. Stephans, S.G. Steadman and W.E. Kehoe; D. Kahana and Y. Torun, *Analysis of Pion Production Data from E-802 at 14.6 GeV/c Using ARC*, BNL-61983 (July 1995); see also http://bnlnth.phy.bnl.gov/arc/arc.html

[11] N.V. Mokhov, *The MARS Code System Usersí Guide*, Fermilab-FN-628 (1995); http://www-ap.fnal.gov/MARS/

[12] N.V. Mokhov and S.I. Striganov, *Model for Pion Production in Proton-Nucleus Interactions*, FERMILAB-Conf-98/053 (Feb. 5, 1998); http://www-lib.fnal.gov/archive/1998/conf/Conf-98-053.html

[13] J. Ranft, *DPMJET version II.3 and II.4*, INFN-AE-97-45 (1997); http://preprints.cern.ch/cgi-bin/setlink?base=preprint&categ=scan&id=SCAN-9711078.

[14] Experiment E-910 at BNL-AGS; http://www.nevis.columbia.edu/heavyion/e910/

[15] *Hadron Production Experiment at the CERN PS*, PS214, http://harp.web.cern.ch/harp/

[16] J. Lettry *et al.*, *Experience with ISOLDE Molten Metal Targets at the CERN-PS Booster*, in Proceedings of ICANS-XIII (1995); http://puhep1.princeton.edu/mumu/target/

[17] G.I. Silvestrov, *Liquid Metal Jet Targets for Intense High Energy Beams*, Budker Institute preprint (Aug. 1998); http://puhep1.princeton.edu/mumu/silvestrov/jet_silvestrov.pdf

[18] C. Johnson, *Solid and Liquid Targets Overview*, Proceeding of the Mini-Workshop: Target and Muon Collection Magnets and Accelerators, (Oxford, MS, 1997, unpublished);
http://nicewww.cern.ch/~cdj/public/mumutarg/
CERN NuFact Jet Target Tests,
http://nicewww.cern.ch/ cdj/public/jet-targ/jet-test.htm

[19] Jack Carpenter, private communication (1996).

[20] J. Walker and W.H. Wells, *Drag Force on a Conducting Spherical Drop in a Nonuniform Magnetic Field*, ORNL/TN-6976 (Sept. 1979).

[21] S. Oshima *et al.*, *The Shape of a Liquid Metal Jet under a Non-uniform Magnetic Field*, JSE Int. J. **30**, 437 (1987),
http://www.hep.princeton.edu/~mcdonald/mumu/target/oshima

[22] C. Lu and K.T. McDonald, *Low-Melting-Temperature Metals for Possible Use as Primary Targets at a Muon Collider Source*, Princeton/$\mu\mu$/97-3 (1998);
http://puhep1.princeton.edu/mumu/mumu-97-3.ps

[23] R. Weggel, *Behavior of Conducting Solid or Liquid Jet Moving in Magnetic Field: 1) Paraxial, 2) Transverse, 3) Oblique*, CAP-220-MUON-98R (1998),
http://www.hep.princeton.edu/~mcdonald/mumu/target/metaljet.pdf

[24] R.B. Palmer and R. Fernow. *Target and Pion Production*, Chap. 2 of *Beam Physics for Muon Colliders*, a course presented at the Accelerator School (Vanderbilt U., Jan. 25-29, 1999),
http://pubweb.bnl.gov/people/palmer/course/2target.ps

[25] R.B. Palmer, *First prder perturbative calculations for a conducting liquid jet in a solenoid*, draft 3 (Oct. 11, 2000),
http://pubweb.bnl.gov/people/palmer/notes/jet.ps

[26] K.T. McDonald, *Damping of Radial Pinch Effects*, Princeton/$\mu\mu$/00-26 (Oct. 31, 2000),
http://www.hep.princeton.edu/~mcdonald/mumu/target/radialpinch.ps

[27] P. Thieberger, *Estimated perturbations of the axial motion of a liquid-metal jet entering a strong magnetic field*, MUC-0182 (Nov. 4, 2000),
http://www-mucool.fnal.gov/mcnotes/muc0182.pdf

[28] K.T. McDonald, *Magnetohydrodynamics of a Continuous Mercury Jet Coaxially Entering a Solenoid*, Princeton/$\mu\mu$/00-29 (Nov. 24, 2000),
http://www.hep.princeton.edu/~mcdonald/mumu/target/continuousjet.ps

[29] C. Lu and K.T. McDonald, *Flowing Tungsten Powder for Possible Use as the Primary Target at a Muon Collider Source*, Princeton/$\mu\mu$/98-10 (Mar. 15, 1998);
http://puhep1.princeton.edu/mumu/mumu-98-10.ps

[30] B.J. King, N.V. Mokhov and R. Weggel, *A Cu-Ni Rotating Band Target for Pion Production at Muon Colliders*, http://pubweb.bnl.gov/people/bking/target_aps98/index.html

[31] J.R.J. Bennett, *A High Power, Radiation Cooled Rotating Toroidal Target for Neutrino Production* (Jan. 19, 2000), http://www.hep.princeton.edu/~mcdonald/mumu/target/bennett_011900.pdf

[32] P. Drumm, *RAL Target Studies*, presented at NuFact'00 (May 23, 2000), http://www.lbl.gov/Conferences/nufact00/docs/WG4_0523_Drumm_SC.pdf

[33] M.A. Green, *Possible Target Otions*, presented at the Orcas Island Workshop (May 1997), http://www.hep.princeton.edu/~mcdonald/mumu/target/Target_Issues.pdf

[34] *Target System and Support Facility*, Chap. 4 [4], http://www.fnal.gov/projects/muon_collider/nu/study/report/machine_report/04_source_target+_re

[35] A. Hassanein *Preliminary Analysis of Target Response to Beam Deposition* (Apr. 2000, http://www.hep.princeton.edu/~mcdonald/mumu/target/AH=Fermi=Report.pdf

[36] A. Abramov *et al.*, *Dynamic Stress Calculations for the NUMI Target*, NuMI-B-675 (Aug. 10, 2000), http://www.hep.anl.gov/ndk/postscript/numib675.ps

[37] B. Riemer, *Graphite Rod Test/Simulation Response from LANSCE-WNR Proton Beam* (Oct. 3, 2000), http://www.hep.princeton.edu/~mcdonald/mumu/target/graphite-lansce.pdf

[38] G.S. Bauer, *ESS Liquid Metal Target Studies*, ESS 95-33-T (Oct. 1995).

[39] G.S. Bauer, *Mercury as a Target Material for Pulsed (Fast) Spallation Neutron Sources*, ICANS-XIII, PSI-Proceedings 95-02 (Oct. 1995), p. 547.

[40] B.R. Appleton and G.S. Bauer, *Proc. Int. Workshop on the Technology and Thermal Hydraulics of Heavy Liquid Metals (Hg, Pb, Bi and Their Eutectics)*, (Schruns, Austria, Mar. 1996), ORNL CONF-9603171 (June 1996).

[41] T.A. Broome, *High Power Targets for Spallation Sources* Proc. EPAC96 (Sitges, Spain, 1996), p. 267; http://www.cern.ch/accelconf/e96/PAPERS/ORALS/TUY04A.PDF

[42] T.A. Gabriel *et al.*, *The National Spallation Neutron Source Target Station: A General Overview*, Proc. PAC97 (Vancouver, 1997), p. 86; http://www.triumf.ca/pac97/papers/pdf/2B012.PDF

[43] *Target Systems*, Chap. 5 of the National Spallation Neutron Source Conceptual Design Report (NSNS/CDR-2, May 1997); http://www.ornl.gov/~nsns/CDRDocuments/CDRSections/Sect5.pdf

[44] J.R. Haines, *Comparison of Liquid and Solid Targets for Pulsed Spallation Neutron Sources*, ORNL report NSNS/TSR0009 (July 1997).

[45] D.B. Cline, ed., *Proceedings of the High Intensity Targeting Workshop*, (Fermilab, April 28-30, 1980).

[46] J.A. Hassberger, *Flowing Liquid Lithium Target*, in [45], p. 12.

[47] R.J. Stefanski, *A Study in Target Design*, in [45], p. 41.

[48] *Feasibility Study into the Development of a Liquid Metal Pulsed Current Target for ACOL*, Report No. C2365/F, Contract No: R/785.985/PS/AA (Cambridge Consultants Ltd., Cambridge, U.K., 1985).

[49] Z. Tang and K. Anderson, *Shock Waves in $\bar{p}$ Target* Fermilab/TN-1763 (Nov. 1991).

[50] K. Skala and G.S. Bauer, *On the Pressure Wave Problem in Liquid Metal Targets*, ICANS-XIII, PSI-Proceedings 95-02 (Oct. 1995).

[51] R.P. Taleyarkhan, S.H. Kim and J.R. Haines, *Modelling & Analysis of AGS Thermal Shock Experiment*, ORNL report.

[52] R.P. Taleyarkhan, F. Moraga and C.D. West, *Experimental Determination of Cavitation Thresholds in Liquid Water and Mercury*, Proc. 2nd Int. Topical Meeting on Accel. Applications, AccApp'98, (Gatlinburg, TN, Sept. 1998); ORNL report.

[53] R.P. Taleyarkhan *et al.*, *Results of Thermal-Shock Modeling & Analyses for the National Spallation Neutron Source*, in *Proc. Topical Meeting on Nuclear Applications of Accelerator Technology*, (Albuquerque, NM, Nov. 1997), p. 293.

[54] L. Ni and G. Bauer, *Dynamic Stress of a Liquid Metal Target Container under Pulsed Heating*, PSI report (1998);
http://puhep1.princeton.edu/mumu/target/bauer/1.html

[55] P. Sievers and P. Pugnat, *Response of Solid and Liquid Targets to High Power Proton Beams for Neutrino Factories*, NuFact035 (Oct. 12, 2000),
http://nicewww.cern.ch/~molat/neutrino/nf35.pdf

[56] J.R. Haines, *A Simple figure of Merit for Comparison of Thermal Shock Capabilities of Candidate Target Materials*, ORNL report NSNS/TSR5 (Mar. 3, 1997).

[57] D.H. Trevena, *Cavitation and Tension in Liquids* (Adam Hilger, Bristol, U.K., 1987).

[58] F.R. Young, *Cavitation* (McGraw-Hill, New York, 1989).

[59] T.G. Leighton, *The Acoustic Bubble* (Academic Press, San Diego, 1994).

[60] H. Maris and S. Balibar, *Negative Pressures and Cavitation in Liquid Helium*, Physics Today (Feb. 2000), p. 29,
http://www.hep.princeton.edu/~mcdonald/mumu/target/bubble.html

[61] A. Kovacs, *Estimating the Full-Scale Tensile, Flexular and Compressive Strength of First-Year Ice*, CRREL Report 96-6 (Sept. 1996), Fig. 9;
http://www.crrel.usa.ce.army.mil/techpub/CRREL_Reports_web/reports/CR96_11.pdf

[62] L. Briggs, *Limiting Negative Pressure of Water*, J. Appl. Phys. **21**, 721 (1950).

[63] D.A. Wilson, J.W. Hoyt and J.W. McKane, *Measurement of tensile strength of liquids by an explosion technique*, Nature **253**, 723 (1975).

[64] *Design Report TEVATRON 1 Project*, Fermilab (Sept. 1984).

[65] R. Criss and F.E. Rose, *Spatial and Temporal Development of Emissions from an Exploding Mercury Jet*, IEEE Trans. Plasma Sci. **23**, 145 (1995).

[66] W.E. Ansley, S.A. Merryman and F.E. Rose, *Characterization of Liquid Mercury Jets and the Potential Application as an Opening Switch*, (1995).

[67] W.E. Ansley and F.E. Rose, *Evaluation of Liquid-Metals Jets as the Conductor in a Rep-Rated, Exploding-Fuse Opening Switch*, IEEE Trans. Magnetics **32**, 1980 (1996).

[68] J. Lettry *et al.*, article in preparation (1998).

[69] H. Ullmaier and E. Carsughi, *Radiation damage problems in high power spallation neutron sources*, Nucl. Instr. and Meth. **B101**, 406 (1995).

[70] T.W. Eaton *et al.*, *Conducting Targets for $\overline{p}$ Production of ACOL. Past Experience and Prospects*, IEEE Trans. Nuc. Sci. **NS-32**, 3060 (1985).

[71] *Autopsie d'Une Cible en Cuivre*, CERN Central Workshop Metallurgy Dept. Report No. 3103 (1984).

[72] *Etude d'Une Cible a Antiprotons en Plomb*, CERN Central Workshop Metallurgy Dept. Report No. 3198 (1984).

[73] *Metallographic Examination of a Lightly Irradiated Copper/Graphite/Aluminium Target for CERN*, Report No. EIR KT: 7.423.0284, Federal Institute for Reactor Research (Wr̈enlingen, Switzerland, 1984).

[74] R. Horne, *Preliminary Post-Irradiation Examination of a Rhenium "Snout" Target*, CERN Remote Handling Section (1985), unpublished; copy with C. Johnson).

[75] *High Temperature Compatibility Between Materials for Pulsed Current Targets*, Report No. OEFZS-A-0852 WE-402/86 (Osterreichisches Forschungzentrum, Seibersdorf, Austria, 1986).

[76] S.C. O'Day and F.M. Bienosek, *8-9 GeV $\bar{p}$ yield measurements at the Fermilab antiproton source*, Nucl. Instr. and Meth. **A343**, 343 (1994).

[77] Al Pendzick, private communication (1998).

[78] Helge Ravn, private communication (1998).

[79] Günter Bauer, private communication (1998).

[80] R.N. Lyon (ed.), *Liquid Metals Handbook*, 2nd ed., NAVEXOS-P.733 (June 1952, revised 1954); *Liquid Metals*, in *Reactor Handbook*, 2nd ed., C.R. Tipton, Jr., (ed.), Interscience, New York, 1960), p. 994.

[81] *Materials for Spallation Neutron Sources*, Proceedings of the Workshop held at Los Alamos National Laboratory (Feb. 6-10, 1995), ed. by A. Longshore, LA-13097; http.//lib-www.lanl.gov/la-pubs/00285851.pdf

[82] J.R. DiStefano, *A Review of the Compatibility of Containment Materials with Potential Liquid Metal Targets*, ORNL-TM-13056 (Aug. 1995).

[83] D. Filges, R.D. Neef and H. Schaal, *Nuclear Studies of Different Target Systems for ESS*, ICANS-XIII, PSI-Proceedings 95-02 (Oct. 1995), p. 537.

[84] L. Briggs, *Limiting Negative Pressure of Mercury in Pyrex Glass*, J. Appl. Phys. **24**, 488 (1953).

[85] A. des Brasunas, *Interim Report on Static Liquid-Metal Corrosion*, ORNL/TM1646 (May 11, 1954).

[86] J.V. Cathcart and W.D. Manly, *The Mass Transfer Properties of Various Metals and Alloys in Liquid Lead*, Corrosion **12**(2), 43 (Feb. 1956).

[87] A.J. Romano, C.J. Kamut and D.H. Gurinsky, *The Investigation of Container Materials for Bi and Pb Alloys. Part I. Thermal Convection Loops*, BNL-811 (T-313) (July 1963).

[88] G.M. Tolsen and A. Taboda, *A Study of Lead and Lead-Salt Corrosion in Thermal-Convection Loops*, ORNL/TM-1437 (April 1966).

[89] J.R. Weeks, *Lead, Bismuth, Tin and Their Alloys as Nuclear Coolants*, Nucl. Eng. and Des. **15**, 363 (1971).

[90] J.R. DiStefano and O.B. Cavin, *Temperature Gradient Compatibility Tests of Some Refactory Metals and Alloys in Bismuth and Bismuth-Lithium Solution*, ORNL/TM-5503 (Nov. !976).

[91] H. Baker (ed.), *Alloy Phase Diagrams*, 2nd ed., Vol. III of the ASM handbook (ASM International, Materials Park, OH, 1997).

[92] J. Yahia and J.P. Thobe, *The Temperature Dependence of the Resistivity of Liquid Gallium to 1000°C*, Can. J. Phys. **50**, 2554 (1972).

[93] R.K. Smither *et al.*, *Liquid gallium cooling of silicon crystals in high intensity photons beams*, Rev. Sci. Instr. **60**, 1486 (1989).

[94] R.K. Smither *et al.*, *Recent experiments with liquid gallium cooling of crystal diffraction optics*, Rev. Sci. Instr. **63**, 1746 (1992).

[95] Lord Rayleigh, *The Theory of Sound* (reprinted by Dover, 1945), Vol. 2, p. 362.

[96] S. Chandrasekhar, *Hydrodynamic and Hydromagnetic Stability* (reprinted by Dover, 1981), §112.

[97] J.D. Jackson, *Classical Electrodynamics* (Wiley, New York, 1975), 2nd ed., chap. 10.